LITHOS 514-515 (2025) 108197

Contents lists available at ScienceDirect

LITHOS

journal homepage: www.elsevier.com/locate/lithos

Zircon records water-fluxed melting in origin of W-rich magma: Insights from the Yangchuling porphyry W—Mo deposit, South China

Qingqing Yin [a,b], Juxing Tang [a,b,*], Jingjing Dai [a,*], Inna Safonova [b,c], Faqiao Li [a], Hao Sun [a], Yumin Xu [d], Xinkui Xiang [d], Jinling Xie [b,a], Baoping Gan [b,a], Bohao Yin [e], Zhongchao Zheng [f], Feng Liang [a], Liqiang Wang [a]

[a] State Key Laboratory of Deep Earth and Mineral Exploration, Institute of Mineral Resources, Chinese Academy of Geological Sciences, Baiwanzhuang Street 26, Beijing 100037, China
[b] Faculty of Geosciences and Engineering, Southwest Jiaotong University, Xi'an Road 999, Chengdu 611756, China
[c] Sobolev Institute of Geology and Mineralogy, SB RAS, Koptyuga ave. 3, Novosibirsk 630090, Russia
[d] The Third Geological Brigade of Jiangxi Geological Bureau, South Lushan Road 109, Jiujiang 332100, China
[e] School of Earth System Science, Tianjin University, Wejin Road 92, Tianjin 300072, China
[f] The Eighth Geological Brigade of Jiangxi Geological Bureau, Daihu Road 56, Shangrao 334001, China

ARTICLE INFO

Keywords:
W-rich granitoids
Zircon geochemistry
U-Pb zircon ages
Re-Os molybdenite ages
Whole-rock geochemistry

ABSTRACT

Generation of W-rich magma is generally associated with dehydration melting of mica-bearing supracrustal metasedimentary rocks. However, it remains uncertain whether a water-fluxed melting of infracrustal rocks can also produce W-rich magma. In this paper, we present new data on the geochemistry of zircons, whole-rock composition of granitoids, and *Re*—Os isotope systematics of molybdenite from W—Mo orebodies of the Yangchuling-Guaishan area located in the central part of the world-class Jiangnan Tungsten Ore Belt (JTOB). Compared with the S-type W-rich granitic magmas of the whole JTOB, the I-type granitic magmas of the Yangchuling deposit were more H_2O-saturated and could easily ascend in a decompressional setting. The input of mantle-derived melts weakened the fertility of the late-stage granites. During the crystallization of zircon, the I-type granitic magmas that produced the Yangchuling W—Mo deposit possessed moderately reductive characteristics, similar to those of the S-type granitic magmas of the large deposits in the JTOB. The magmas associated with the large-scale W—Sn polymetallic mineralization in the JTOB appear to be of crustal origin. At early stages, the water-fluxed melting triggered the formation of low-T, high-silica fertile and H_2O-saturated magmas, which could ascend more easily compared to those that produced the later barren magmatic rocks. At the late stage, the potential of W-mineralization in the Yangchuling-Guaishan area decreased, probably due to the increased contribution of the mantle-derived melts. Extensional thinning of the crust accelerated magma ascent, suppressed magmatic residence time, limited fractionation, and reduced volatile enrichment in the Yangchuling W—Mo deposit. Conclusively, we suggest that the water-fluxed melting played a key role in the generation of W-rich magma.

1. Introduction

The Jiangnan Tungsten Ore Belt (JTOB) hosts several huge tungsten ore deposits, including the world-class Dahutang and Zhuxi deposits, as well as the large-scale Yangchuling deposit. Recently, a series of new W deposits associated with I-type granites have been explored in the eastern JTOB. Both oxidized I-type and reduced S-type granitic magmas can produce tungsten mineralization (Xiang et al., 2015; Mao et al., 2020; Yin et al., 2020; Zhang et al., 2021; Song et al., 2023). I-type and S-type granites originate from distinct crustal sources: I-type from biotite-rich intracrustal reservoirs, and S-type from muscovite or two-mica-rich supracrustal source regions (Sant Ovaia et al., 2021). Large tungsten deposits, e.g., Dahutang, Zhuxi, Xihuashan and Shizhuayuan (Jiang et al., 2019; Shen et al., 2022; Yin et al., 2025; Zhang et al., 2020), mainly derive from the latter source due to its abundance of W-host minerals (e.g., biotite, titanite and rutile; Romer and Kroner, 2016).

* Corresponding authors at: State Key Laboratory of Deep Earth and Mineral Exploration, Institute of Mineral Resources, Chinese Academy of Geological Sciences, Baiwanzhuang Street 26, Beijing 100037, China.
E-mail addresses: tangjuxing@126.com (J. Tang), daijingjing863@sina.com (J. Dai).

https://doi.org/10.1016/j.lithos.2025.108197
Received 21 January 2025; Received in revised form 23 July 2025; Accepted 23 July 2025
Available online 24 July 2025

Water is crucial in the generation of W-rich magma derived from both types of magmatic sources, intracrustal and supracrustal. The sources and content of water in the magma source region influence diagenetic temperature, melting reaction (water-fluxed or dehydration melting), degree of melting, melt H_2O saturation, granitic volume, and even the exsolution of W-bearing fluids during the late magmatic stage (Collins et al., 2020; Ge et al., 2023; Romer and Kroner, 2016; Weinberg and Hasalová, 2015; Zhao et al., 2022b). The presence of replenished external water determines whether water-fluxed melting or dehydration melting occurs (Weinberg and Hasalová, 2015). Dehydration melting of muscovite (or two-mica) in supracrustal metasedimentary rocks can generate W-rich magma, as confirmed by numerous previous studies (Romer and Kroner, 2016; Roy et al., 2024; Yuan et al., 2019; Zhao et al., 2022a). However, whether water-fluxed melting in intracrustal rocks triggered by deep recycled water can generate W-rich magma remains uncertain.

Located 17 km northeast of Duchang County (Jiangxi Province, China), the Yangchuling porphyry W—Mo deposit (>6.06 Mt. WO_3 proven) occupies the central region of Jiangnan Tungsten Ore Belt (JTOB; Fig. 1) (Mao et al., 2020). It represents one of the few large-scale tungsten systems globally associated with I-type granites (Mao et al., 2017; Song et al., 2023). In the Yangchuling-Guaishan area, five granitoid groups, including two newly identified in this study, and synplutonic spessartite dikes are characterized by a temporally continuous emplacement and spatially cross-cutting relationships (Fig. 2–3). These magmas exhibit a gradual evolution from granitic to granodioritic melts, characterized by a distinct trend of silicon reduction, in contrast to the typical crystallization differentiation process that leads to high-silica

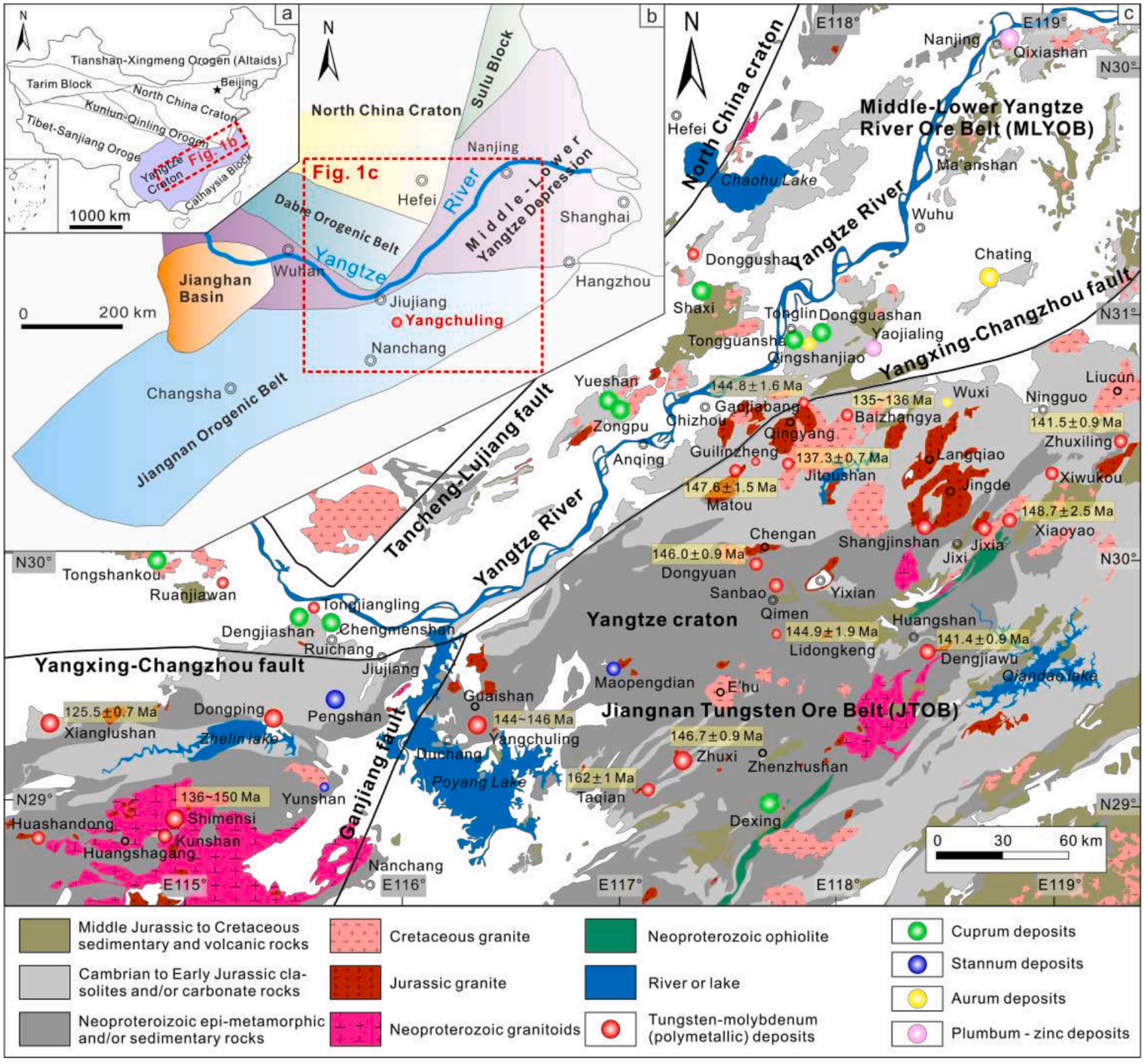

Fig. 1. Tectonic map of China showing the main tectonic units and the Yangtze blocks in South China (a); Distribution of tectonic units in South China, showing the location of the Middle-Lower Yangtze River depression and the Jiangnan Orogenic Belt (JOB) (b); Summary geological map of the Jiangnan Tungsten Ore Belt (JTOB) and the Middle-Lower Yangtze River ore belt, showing the distribution of the W, Cu, Sn, Au, and Pb—Zn deposits (c) (modified after Wang et al., 2023 and Mao et al., 2017).

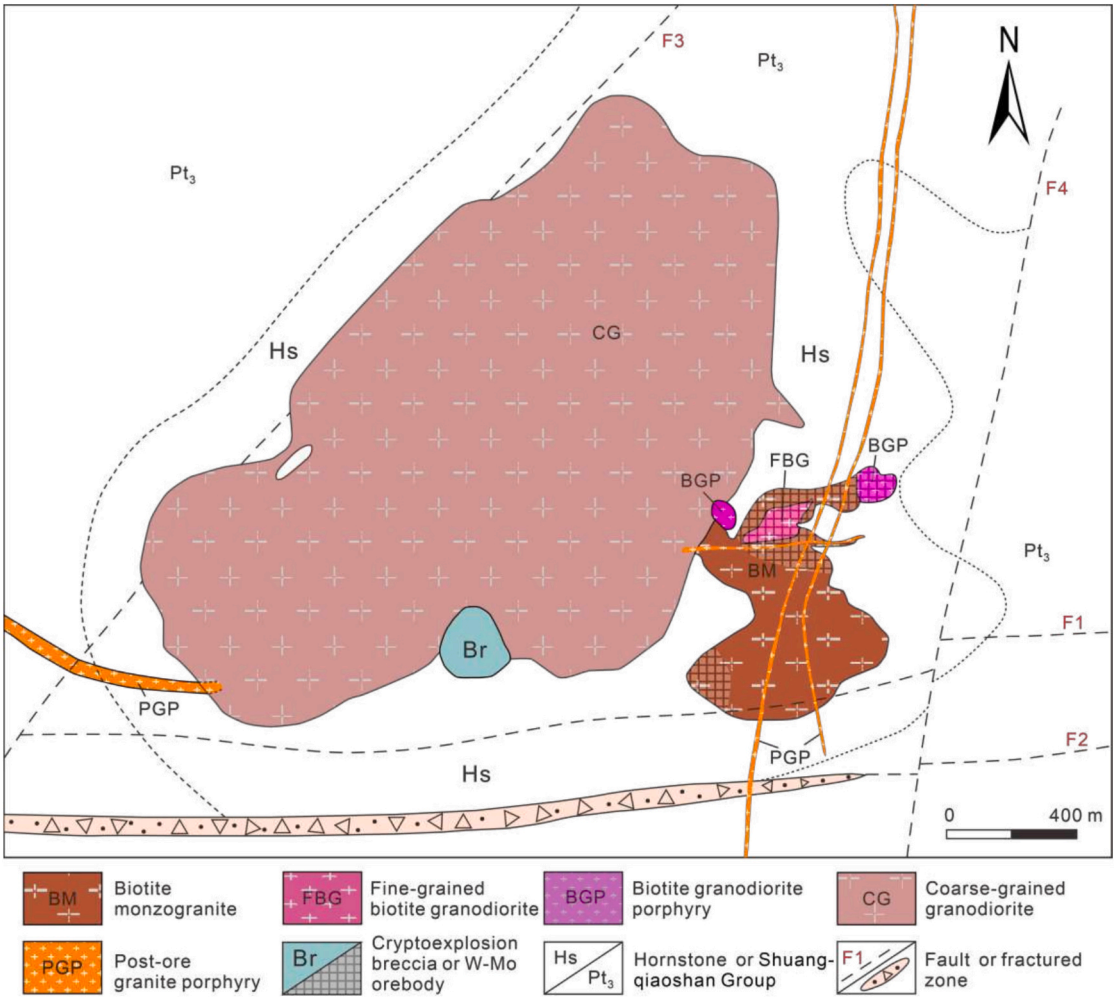

Fig. 2. Outline map of the Yangchuling W—Mo deposit (modified after Xu et al., 2023).

compositions. The mantle-derived component likely plays a significant role in the intermediate-acidic trend of reverse evolution within the magmatic sequence. These Mesozoic magmatic sequences from the Yangchuling W—Mo deposit in the Jiangnan Orogenic Belt preserve a complete record of deep-seated melting processes driving W-enrichment and constitute an ideal natural laboratory for tungsten-rich magma genesis studies. The ways of partitioning trace elements into zircon during crystallization are highly sensitive to the content of water in the melt, oxygen fugacity (f_{O2}), melting temperature, and contribution of mantle materials. All these factors make the trace element composition of zircon a valuable tool for understanding the origin and evolution of W-rich magma (Carrasco-Godoy et al., 2024; Ferry and Watson, 2007; Loader et al., 2017; Loucks et al., 2020; Loucks and Fiorentini, 2023; Mole et al., 2021; Nathwani et al., 2024; Smythe and Brenan, 2015; Yin et al., 2024).

In this paper, we present zircon U—Pb isotope ages and molybdenite *Re*—Os isotope ages to constrain the timing of diagenesis and metallogeny, respectively. We have also conducted trace element compositions of zircons and major and trace element analyses of whole-rock samples from six granitoid groups in the Yangchuling-Guaishan area, central JTOB, to reconstruct the sources of W-rich magma, status of water saturation condition (H_2O-saturated or H_2O-undersaturated), melting reactions (water-fluxed melting vs. dehydration melting), and tectonic regimes.

2. Overview of regional geology

The Jiangnan Orogenic Belt (JOB) extends from Guangxi to Jiangsu situated between the Yangtze and the Cathaysian blocks (Fig. 1b). The Jiangnan Tungsten Ore Belt (JTOB) is in the middle and eastern segments of Jiangnan Orogenic Belt (Fig. 1c). Two distinct types of Mesozoic granites are associated with the tungsten polymetallic mineralization in the JTOB: I-type granitoids (e.g., Zhuxiling, Dengjiawu, and Yangchuling) and S-type granitoids (e.g., Dahutang and Zhuxi) (Fig. 1c), the latter contribute the primary tungsten budget (Mao et al., 2020).

The Yangchuling deposit hosts large-scale reserves of tungsten and molybdenum (Xu et al., 2023). The Yangchuling deposit is classified as a quartz-veinlet type mineralization deposit (Mao et al., 2017; Song et al., 2023; Xu et al., 2023). The Mesozoic granites intrude the Anlelin Formation of the Shuangqiaoshan Group, which forms the country rock (Fig. 2). The quartz veinlet clusters occur proximally to the base of the Proterozoic meta-sedimentary strata, confined to the inner contact zone between the Anlelin Formation and the Mesozoic intrusions (Xu et al., 2023). Scheelite and molybdenite comprise the predominant ore minerals, with quartz as the dominant gangue phase and late-stage calcite as a subordinate gangue component. Hydrothermal alteration at Yangchuling progresses through distinct stages: (1) potassic alteration, (2) greisenization, (3) chloritization and (4) carbonation alteration systems (Xu et al., 2023). The Yangchuling Mesozoic intrusions predominantly consist of high-K calc-alkaline granites, which include biotite monzogranite (BM, Fig. 3a, c, g), fine-grained biotite granodiorite

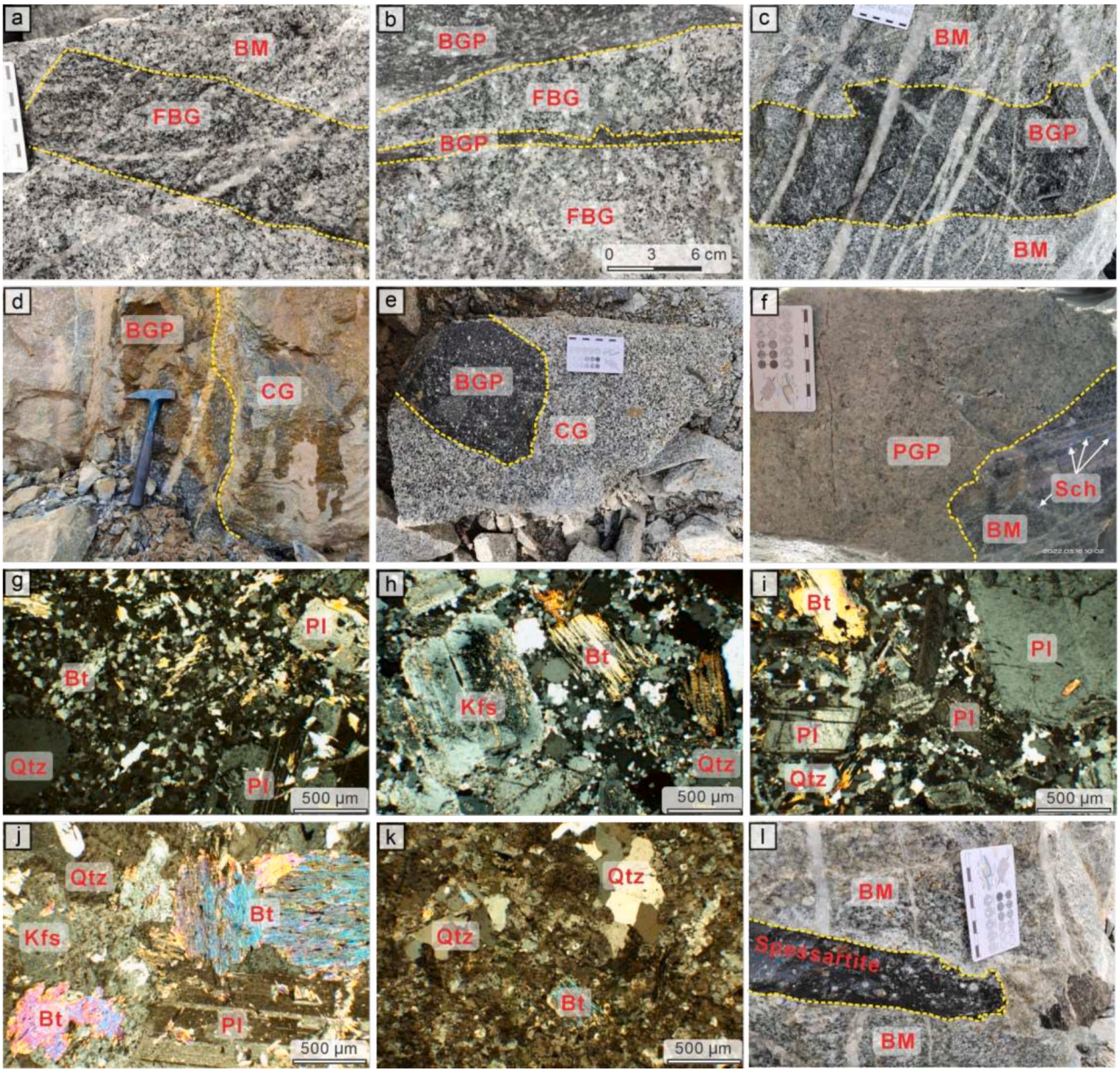

Fig. 3. Representative specimens and photomicrographs of granites and spessartite of the Yangchuling W—Mo deposit: (a) an intrusion of fine-grained biotite granodiorite into biotite monzogranite; (b) biotite granodiorite porphyry intrudes into fine-grained biotite granodiorite as a fine vein, and the ore-bearing quartz vein in fine-grained biotite granodiorite are crosscut by biotite granodiorite porphyry; (c) biotite granodiorite porphyry intrudes into biotite monzogranite, and ore-bearing quartz veins penetrate both; (d) at the boundary of the biotite granodiorite porphyry and the coarse-grained granodiorite, a quartz vein hosted in the former is crosscut by the latter; (e) biotite granodiorite porphyry occurs as xenoliths in coarse-grained granodiorite; (f) at the boundary of the biotite monzogranite and the post-ore granite porphyry, ore-bearing quartz veins hosted in the former is crosscut by the latter; (g-k) photomicrographs of biotite monzogranite (BM), fine-grained biotite granodiorite (FBG), biotite granodiorite porphyry (BGP), coarse-grained granodiorite (CG), and post-ore granite porphyry (PGP), respectively; (i) the ore-bearing quartz veins in biotite monzogranite are crosscut by an intrusive vein of spessartite. Mineral abbreviations: Qtz = quartz, Pl = plagioclase, Kfs = K-feldspar, Bt = biotite, Sch = scheelite, Mol = molybdenite.

(FBG, Fig. 3a, b, h), biotite granodiorite porphyry (BGP, Fig. 3b-e, i), coarse-grained granodiorite (CG, Fig. 3d, e, j), and post-ore granite porphyry (PGP, Fig. 3f, k), spanning early to late stages. W—Mo mineralization is associated with the BM and FBG granites, while weak mineralization occurs in the BGP and CG granites. The PGP granite is identified as a barren post-mineralization intrusion (Fig. 3f). The latest phase of synplutonic spessartite dikes cut through the five early granitoids and W—Mo orebodies (Fig. 3l).

3. Methods

3.1. Sampling

The Ganjiang fault, a trans-crustal scale structure (Cao et al., 2022), may have segmented the deep W-rich source within the JTOB (Fig. 1c). In terms of the two types of Mesozoic W-rich S- and I-type granites in the JTOB, acidic S-type granites occurring the west of the Ganjiang fault are more peraluminous and highly differentiated than intermediate-acidic I-type granites to the northeast. The multiple intrusions of the Yangchuling W—Mo deposit mark a significant milestone in the study of tungsten-mineralized magmas within the JTOB, as it represents the first

documented spatial occurrence of a W-rich I-type granitic magmatic system east of the Ganjiang fault. Our drilling investigation revealed that the CG granite, which intruded into the Yangchuling deposit, also intruded beneath the Guaishan area, exhibiting only weak molybdenum mineralization but no scheelite mineralization. Zircon samples were therefore collected from both the multiple intrusions of the Yangchuling deposit and the CG granite of the Guaishan area, along with molybdenite samples, to assess the timing and potential of tungsten mineralization.

3.2. Whole-rock composition analysis and molybdenite Re—Os isotope dating

Major and trace element analyses were performed at Ausilicon Analytical Testing (Guangzhou) Co., Ltd. Major elements were determined by wavelength-dispersive X-ray fluorescence spectrometry (XRF) using fused lithium borate beads (Method P61-XRF15b; precision better than 5 %). Rare earth elements (REE) were analyzed by inductively coupled plasma-mass spectrometry (ICP-MS) following lithium metaborate fusion (Method ME-MS81; precision better than 10 %). The content of FeO was quantified through potassium dichromate titration (Method Fe-VOL05; precision better than 3.54 %). All results of whole-rock composition are presented in Supplementary Table S1. Molybdenite Re—Os isotope analyses were performed at the National Geological Experiment and Testing Center. Following sample decomposition, osmium tetroxide (OsO_4) vapor was trapped by aqueous absorption for Os isotope ratio analysis. The residual solution was transferred to a Teflon beaker for subsequent Re separation. This residue was evaporated to near-dryness, alkalinized with 10 mol/L NaOH (pH adjusted), and subjected to methyl ethyl ketone (MEK) extraction via centrifugal oscillation. The organic phase was transferred to a Teflon beaker, with solvents volatilized at 50 °C followed by drying at 120 °C. *prior* to final drying, residual Os was eliminated by dropwise addition of H_2O_2 and concentrated HNO_3. The resulting residue was dissolved in HNO_3 for Re isotope ratio determination using an X-Series ICP-MS. Detailed procedures follow Du et al. (2012).

3.3. Zircon U—Pb isotopes and trace elements

Six granite samples were collected from the Yangchuling-Guaishan area for zircon chronology and mineralogical studies (Fig. 1). The separated zircons were encapsulated in epoxy and polished to a thickness of 20 μm. Ablation sites were selected based on cathodoluminescence (CL) petrography to ensure sites were in zones of oscillatory growth associated with magmatic origins (Fig. S1) (Hoskin, 2005). Isotopes and elements were analyzed simultaneously by LA-ICP-MS at the Institute of Mineral Resources, Chinese Academy of Geological Sciences. NIST610 glass and ^{91}Zr were used as external and internal standards, respectively. Blank signal, element content, and isotopic calculations were selected using the ICPMSDATACAL program (Liu et al., 2008). The dating diagrams were plotted using the software "IsoplotR" (Vermeesch, 2018).

3.4. Estimates of zircon geochemistry index

To eliminate inherited zircons, only U—Pb dating grains considered temporally compatible were selected for trace element analysis based on three criteria—LREE Index (LREE-I) $>$ 10, Ti $<$ 50 ppm, and La $<$ 1 ppm—to minimize the effects of hydrothermal alteration, inclusions and inherited cores on analytical ablation spot (Bell et al., 2016, 2019; Loucks et al., 2020). In parental magma, the trace element composition of zircon records the physicochemical conditions during crystallization (Loucks et al., 2024; Roberts et al., 2024). Several zircon oxy-barometry methods have been proposed to estimate magma f_{O2} (Burnham and Berry, 2012; Loader et al., 2017; Loucks et al., 2020; Smythe and Brenan, 2015; Trail et al., 2012). As heterovalent Ce species are sensitive to f_{O2} variations, the ratio of Ce^{4+}/Ce^{3+}_{zircon} can serve as a semiquantitative proxy for melt f_{O2} during zircon crystallization (Burnham and Berry, 2012; Loader et al., 2017). In this study, both Smythe and Brenan (2015) and Loucks et al. (2020) models were applied to constrain the f_{O2} of W-Sn-rich magma quantitatively. The oxy-barometry of Smythe and Brenan (2015) is primarily based on a calibration model that relates f_{O2} to four parameters: melt composition, H_2O content, temperature ($T_{Ti\text{-}in\text{-}zircon}$) and Ce^{4+}/Ce^{3+}_{melt}. In contrast to the former oxy-barometry (Loucks et al., 2020), the method does not rely on the composition or water content of the parental melt but only considers the amounts of Ti, Ce, and initial U (U_i) in age-corrected zircons.

4. Results

4.1. Chemical composition of granitoid

The whole-rock element compositions of the six granitoid groups from the Yangchuling deposit and Guaishan area are shown in Supplementary Table S1. All of them are weakly peraluminous granitoids with high SiO_2 (66.80–73.53 %), $K_2O + Na_2O$ (6.56–8.53 %) and A/CNK (0.97–1.07) (Fig. S2 a, b). All whole-rock samples exhibit largely parallel pattern curves in Fig. S3, with the CG granodiorites from Yangchuling and the Guaishan showing completely overlapping distribution curves for both REE and trace elements (Fig. S3 a, b). The trace element compositions, along with their consistent structure and major element compositions (Fig. S2), suggest that both the Guaishan CG and Yangchuling CG granodiorites form part of the regional granodiorite batholith. The intermediate Zr concentration and moderately high Ga/Al ratio, combined with the negative correlation trend between P and Si, suggest that all granitoid samples are fractionated I-type granitoids (Fig. S2 c, d). These granitoids differ significantly from the typical highly differentiated granitoids in the Dahutang ore field and exhibit weakly negative anomalies in Eu, Sr and Ba (Fig. S3a, b). The results indicate that the Yangchuling-Guaishan granitoid is a weakly peraluminous I-type granitoid with weak differentiation. Although PGP has the highest SiO_2 content and the lowest $Mg^{\#}$ value (30), this may be attributed to its high degree of differentiation, characterized by a higher differentiation index (DI = 87) and greater depletion of Ti and P (Fig. 4b).

4.2. Zircon and molybdenite dating

This study presents comprehensive dating data for zircons and molybdenites from Yangchuling and Guaishan (Supplementary Table S2 and S3). The six groups of zircons obtained from five sets of Yangchuling granitoids (YCL-11, KD2–4, YCL-1, KD6–4 and KD5–1) and one set from the Guaishan CG granodiorite (GD1–4) morphologically differ from hydrothermal zircon. All of them exhibit clear oscillatory growth zoning, characterized by light to dark gray hues. The six samples yield ages of 143.9 ± 0.8 Ma (YCL-11), 142.8 ± 0.8 Ma (KD2–4), 144.2 ± 0.7 Ma (YCL-1), 143.0 ± 0.6 Ma (KD6–4), 143.3 ± 0.9 Ma (KD5–1) and 143.6 ± 0.6 Ma (GD1–4), respectively (Fig. 4). Their weighted mean ages are consistent with their concordia ages: 143.3 ± 0.8 Ma, 142.4 ± 0.7 Ma, 144.2 ± 0.7 Ma, 142.6 ± 0.6 Ma, 141.7 ± 0.8 Ma, and 143.6 ± 0.6 Ma. Both the Yangchuling and Guaishan CG granodiorites exhibit a consistent mineral composition and coarse-grained porphyritic structure. Moreover, their consistent crystallization times suggest that their emplacement occurred during the same magmatic event. Along with the other four types of intrusive rocks (BM, FBG, BGP, CG and PGP), five magmatic events are identified in the study area. Except for sample KD14–1, the other four molybdenite samples (KD2–3, KD3–3, KD12–1 and KD13–1) from the Yangchuling deposit yield a narrow range of *Re*—Os ages (141.3–144.4 Ma) with a weighted mean age of 143.8 ± 1.9 Ma (Fig. 5). The Re concentrations are predominantly in the range of 41 ppm to 109 ppm, with an average of 52 ppm, which is moderately high (Supplementary Table S3). Five data points with different Re concentrations fit an isochron with a weighted mean age of 143.8 ± 1.9 Ma (Fig. 5). Therefore, mineralization within error is coeval with

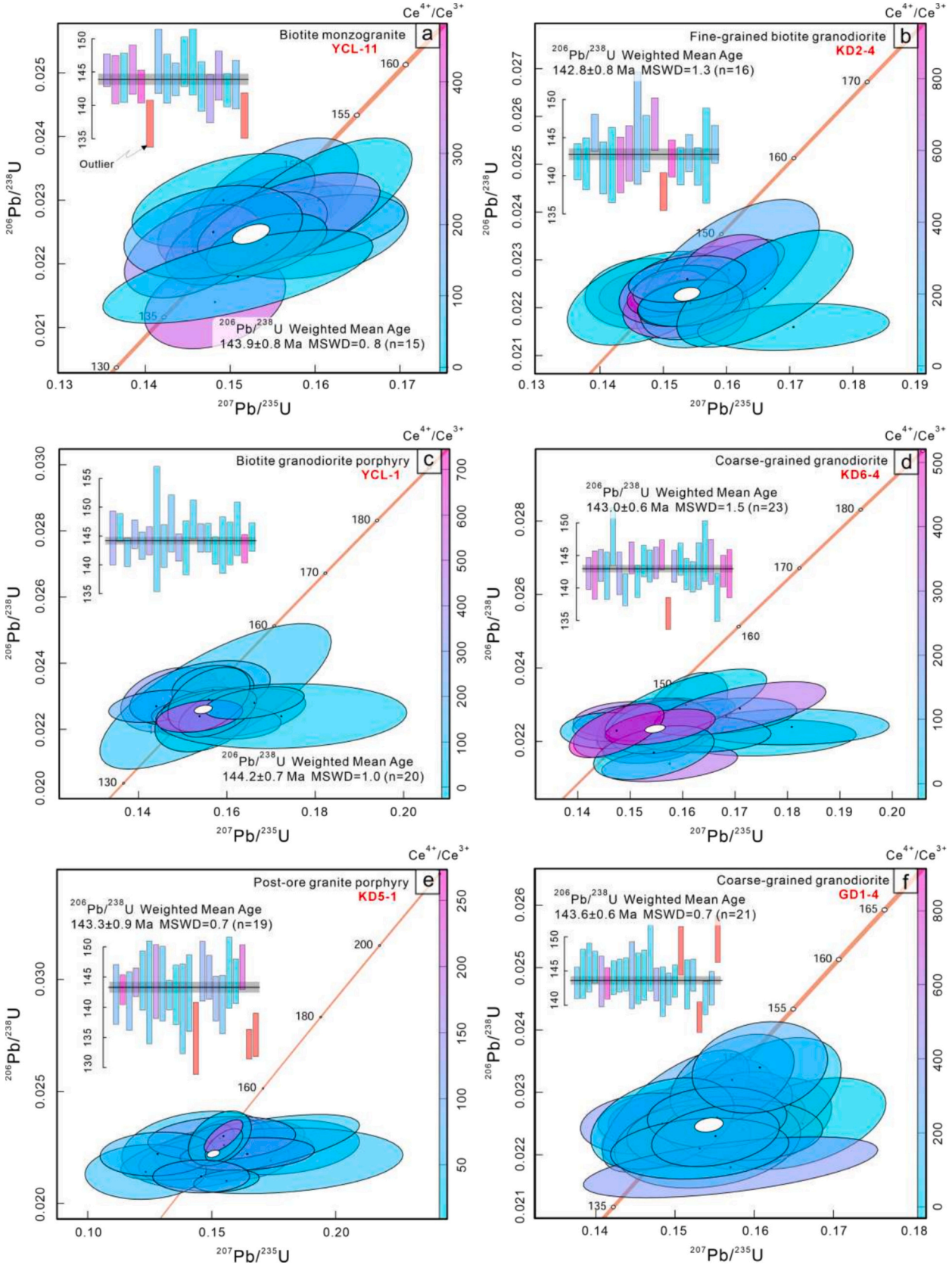

Fig. 4. Zircon U—Pb concordia diagrams for (a) sample YCL-11, (b) sample KD2–4, (c) sample YCL-1, (d) sample KD6–4, (e) sample KD5–1, and (f) sample GD1–4 in the Yangchuling W—Mo deposit and the Guaishan area.

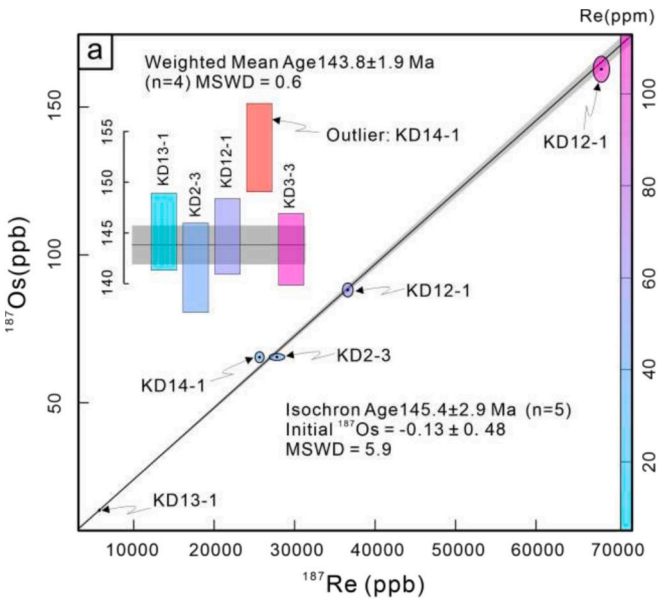

Fig. 5. *Re*—Os isochron and weighted average age diagram for molybdenite from the vein orebody in the Yangchuling deposit.

diagenesis during the Early Cretaceous in the Yangchuling-Guaishan area.

4.3. Zircon composition and oxy-barometry

The chemical compositions of zircons from the Yangchuling and Guaishan granites are listed in Supplementary Table S4. The zircon grains from the Yangchuling and Guaishan areas are identified as magmatic zircons due to their oscillatory zoned structure (Fig. S2) and low light REE (LREE) contents, which are distinctly different from those of hydrothermal zircons (Fig. 6) (Hoskin, 2005). The estimated f_{O2} of the early magma yields a narrow range around the fayalite-magnetite-quartz (FMQ) buffer, using both Smythe and Brenan (2015) and Loucks et al. (2020) models (Fig. 7). The f_{O2} estimated by the oxy-barometry model of Smythe and Brenan (2015) is 0.5 logarithmic units higher than that of the Loucks et al. (2020) model, due to an inaccuracy in the water content of the intrusions. The Loucks et al. (2020) method does not rely on the composition or water content of the parental melt, so the f_{O2} estimation applies the model uniformly for a parallel comparison between the Yangchuling deposit and the Guaishan area.

5. Discussion

5.1. Diagenetic and metallogenic timing

Jurassic-Cretaceous magmatism of the JTOB resulted in the formation of numerous porphyry-skarn W—Sn polymetallic deposits with diverse metallogenic element assemblages, e.g., Dahutang (W-Cu-Mo), Zhuxi (W—Cu), Yangchuling (W—Mo), Xianglushan (W), Pengshan (Sn-Pb-Zn) and Zhuxiling (W—Mo) (Mao et al., 2020; Yin et al., 2024). The previously determined zircon crystallization ages of granitoids range from 144 to 150 Ma, spanning the Late Jurassic to Early Cretaceous (Fan et al., 2022; Mao et al., 2017). In this study, we present six sets of high-precision diagenetic age data and identify five magmatic events. The first four magmatic events are dated to 143.9 ± 0.8 Ma (BM), 142.8 ± 0.8 Ma (FBG), 144.2 ± 0.7 Ma (BGP) and 143.0 ± 0.6 Ma (CG from Yangchuling) and 143.6 ± 0.6 Ma (CG from Guaishan), all of which are associated with W—Mo mineralization. Crosscutting relationships confirm the fifth intrusive phase (143.3 ± 0.9 Ma; PGP) postdates mineralization, as it truncates both the older four granites and W—Mo orebodies. (Fig. 2 and Fig. 3f). Therefore, these five magmatic events occurred over a brief interval (143–144 Ma) during the Early Cretaceous in the Yangchuling-Guaishan area, as shown by our new age-dating data.

Re—Os dating of molybdenite from molybdenite-scheelite-quartz veins constrains the ore-forming age at 143.8 ± 1.9 Ma (MSWD = 0.6) in the Yangchuling deposit, directly timing the mineralizing hydrothermal event. (Fig. 5, Supplementary Table S3). There is a strong agreement between the zircon age of 143–144 Ma and the age of molybdenite Re—Os. Therefore, diagenesis and mineralization occurred nearly simultaneously in the Early Cretaceous. The molybdenite Re—Os ages of the Yangchuling deposit are similar to those of the Dahutang, Zhuxi, Dongyuan, and Matou deposits (Fig. 1, Supplementary Table S3). However, the Re concentrations from the molybdenite of these deposits

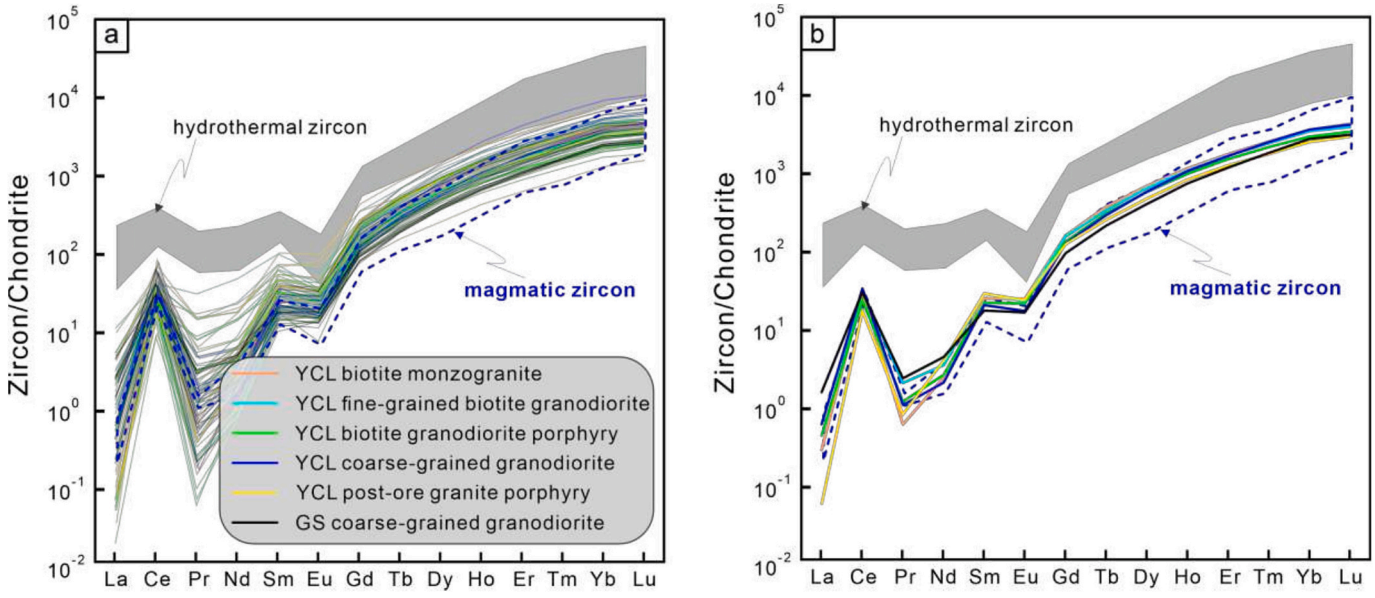

Fig. 6. (a) Chondrite-normalized REE distribution patterns, with normalization values from (Sun and McDonough, 1989) and (b) averaged curves of the corresponding color sample data in zircons from the Yangchuling and Guaishan granites. Note: typical distribution patterns of magmatic and hydrothermal zircons are from (Hoskin, 2005).

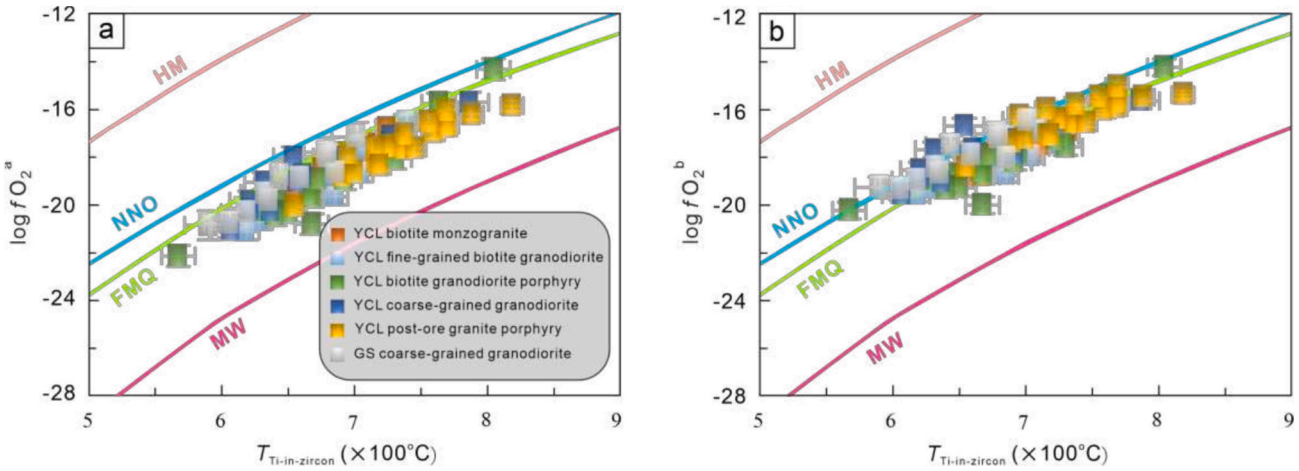

Fig. 7. The relationship between $T_{\text{Ti-in-zircon}}$ versus oxygen fugacity for the Yangchuling and Guaishan granites. The $\log f^{a}_{O2}$ and $\log f^{b}_{O2}$ for zircon, along with gray 2σ error bars, were calculated following (Smythe and Brenan, 2015) and (Loucks et al., 2020), respectively. HM: hematite-magnetite, NNO: nickel-nickel oxide, FMQ: fayalite-magnetite-quartz, MW: magnetite-hematite.

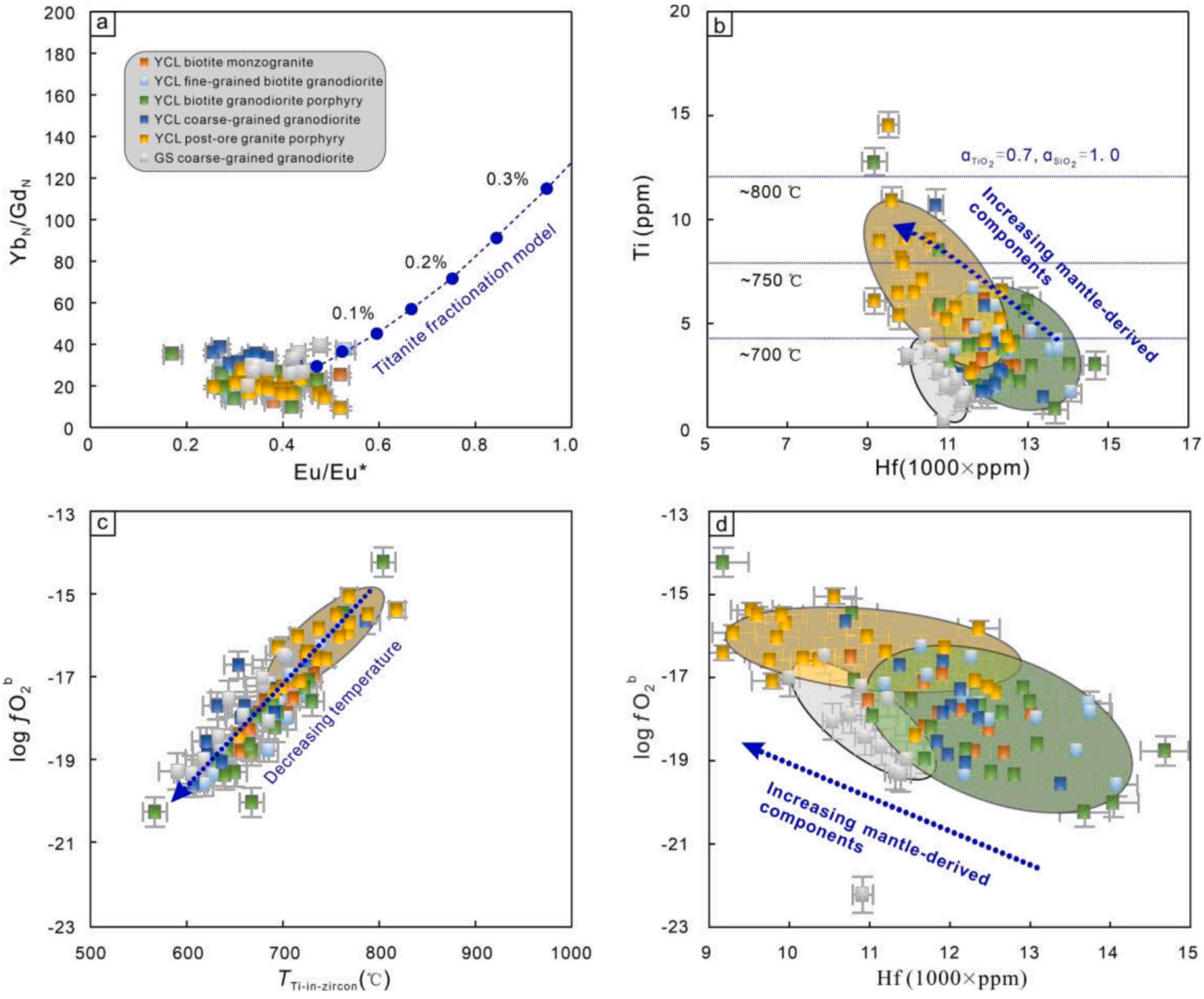

Fig. 8. Plots of Eu/Eu* vs. Yb_N/Gd_N (a), Hf vs. Ti (b), $T_{\text{Ti-in-zircon}}$ vs. $\log f^{b}_{O2}$ (c), and Hf vs. $\log f^{b}_{O2}$ (d) in zircons from the Yangchuling and Guaishan granites. The titanite fractionation curve is from (Loader et al., 2017).

show considerable fluctuations. According to the mass balance model in porphyry-metallogenic systems, Re-rich or Re-poor molybdenum can serve as indicators of specific deposit types (e.g., porphyry Cu—Mo or Climax-type Mo deposits; Stein et al., 2001). Published Re—Os data (Mao et al., 2017; Zeng et al., 2019), along with our new data, indicate that molybdenite from the Yangchuling deposit has moderately high Re concentrations averaging 68 ppm (Supplementary Table S3). Rhenium concentrations in molybdenites are related to the Re source (Mao et al., 1999). The sources of the parental magmas for Xianglushan, Shimensi and Meizikeng are crust-dominated, with low-Re molybdenite (less than 20 ppm; Xiang et al., 2013; Dai et al., 2018; Song et al., 2018), while the formation of the Yangchuling deposit, which contains high-Re molybdenite (more than 20 ppm), may involve a higher proportion of mantle-derived components.

5.2. Hybrid sources of W-rich magma

Generally, metasediment-derived granites have lower Th/U and Ce/U ratios than those derived from the infracrustal melting of enriched basalt owing to relatively reduced conditions and co-crystallizing monazite during zircon crystallization (Foden et al., 2015; Roberts et al., 2024). The Yangchuling and Guaishan granites are classified as 'hybrid' S-type. They are partially located in the overprinting region of 'hybrid' S-type and I-type granites (Fig. 9a). From early to late magmatic stages, the granitic melts exhibit progressively higher Ce/U and Th/U ratios (Fig. 9b), accompanied by decreasing SiO_2 content (averaging from 70.84 % to 67.84 %), increasing MgO content (averaging from 0.84 % to 1.41 %) and increasing $Mg^{\#}$ value (averaging from 38 to 42) (Supplementary Table S1), suggesting that the increasing contribution of mantle-derived components played an important role in the transition from granitic to granodioritic magmas. An increasing degree of differentiation is typically accompanied by increasing Hf content and decreasing titanium saturation temperature in zircon ($T_{Ti\text{-}in\text{-}zircon}$), as shown in Fig. 8b (Samperton et al., 2015). Increasing Hf content and decreasing zircon $T_{Ti\text{-}in\text{-}zircon}$ show a linear tendency toward reducing f_{O2} in each zircon group (Fig. 8c, d). Additionally, the late PGP granite exhibits the highest $T_{Ti\text{-}in\text{-}zircon}$ and f_{O2} in the Yangchuling deposit (Fig. 8b-d), which may indicate the involvement of a larger mantle-source component through extensional thinning (see the following text for details).

Although previous studies classify the granitoids of Yangchuling as I-type (Mao et al., 2017; Song et al., 2023; Xu et al., 2023), the f_{O2} of the early magma exhibits moderate reductive features, similar to those of Dahutang and Zhuxi, characterized by a weak negative value of ΔFMQ. The I-type granitoids from Yangchuling show the opposite characteristic of low f_{O2}, which may be mainly controlled by the composition of the source region. The plot of Nb/Yb vs. U_i/Yb shows that the early BM, FBG and BGP granites originated from 60 % to 70 % mixing with existing crust (Fig. 10a, b), with trends arising from either the depleted mantle (DM) or the primitive mantle (PM) toward evolved upper crust (Mole et al., 2021). The proportion of crustal source components in the Yangchuling granites gradually decreases from early to late stages, as indicated by the blue dotted line in Fig. 10b. The magmas associated with large-scale W—Sn polymetallic mineralization in the JTOB (e.g., Zhuxi, Dahutang and Yangchuling; Zhang et al., 2020; Yin et al., 2025) are typically of high crustal derivation, comprising 60 %–70 % crust-derived components (brown elliptical region, Fig. 10b).

5.3. H_2O-saturated ascent

The average zircon $10^4 \times$ (Eu/Eu*)/Y values of ore-related granites from the Yangchuling deposit (2.13) are consistently higher than those of reductive S-type granites from Shimensi (1.37), Kunshan (0.93) and the Zhuxi deposit (1.47) (Supplementary Table S4) (Lu et al., 2016). This result indicates that I-type granitic magma from the Yangchuling exhibits a highly hydrated nature, significantly more hydrated than S-type granitic magma from the Dahutang and Zhuxi deposits. Notably, a negative correlation between the hydrous indicators of $(Eu/Eu^*)/Yb_N$ and zircon f_{O2} supports a decompressive H_2O-saturated ascent for the parental melt in the Yangchuling W—Mo deposit (Fig. 11d), consistent with similar findings for other porphyry system-related granitoids (Loucks and Fiorentini, 2023). Elevated Rb/Sr ratios (>1) in granitic rocks typically indicate derivation from partial melting of mica-rich metapelitic source region (Castro et al., 1999; Sylvester, 1998). Furthermore, an Rb/Sr ratio of 5 serves as the threshold value demarcating muscovite-dominant versus biotite-dominant partial melting regimes in source terrains (Wang et al., 2003). Samples from the Pengshan and Lianhuashan Sn-enriched magmatic suites exhibit Rb/Sr ratios consistently >5, diagnostic of derivation through partial melting of muscovite (Fig. 12a). In contrast, the Kunshan W-rich magmas at Dahutang display Rb/Sr ratios ranging from 2.17 to 14.15, indicative of partial melting involving both biotite and muscovite breakdown (Fig. 12a).

Water in a magma system typically originates from the dehydration of hydrous minerals or the incorporation of external water (Brown, 2013; Collins et al., 2020). Granitic rocks from Kunshan (Dahutang), Maopengdian (Lianhuashan) and Pengshan exhibit a negative Rb/Sr-Ba correlation diagnostic of muscovite-dehydration melting (Fig. 12a). In contrast, Yangchuling samples display tightly clustered Rb/Sr ratios across variable Ba concentrations, closely resembling H_2O-fluxed melting trends (Inger and Harris, 1993) (Fig. 12b). In addition, Fig. 12c further highlights the petrogenetic divergence of Yangchuling samples, manifesting low-Rb/high-Sr signatures diagnostic of H_2O-fluxed melting. This contrasts sharply with the high-Rb/low-Sr fingerprint characteristic of dehydration melting established across other sample suites (Gao et al., 2017). The W-Mo-rich I-type granites from the Yangchuling and Zhuxiling deposits originated through H_2O-fluxed melting, whereas the W-rich S-type granites from the Shimensi and Kunshan deposits, characterized by lower FeO content and Na_2O/K_2O ratios, formed via dehydration melting (Fig. 12d; Weinberg and Hasalová, 2015).

Furthermore, the lower $T_{Ti\text{-}in\text{-}zircon}$ values provide evidence supporting the involvement of external water in the generation of the W-Mo-rich magma in the Yangchuling deposit. An increase of 1 wt% in water content within the source region would decrease the melting temperature by ~30 to 150 °C (Ge et al., 2022). The presence of external water lowered the solidus temperature of the source components, enabling partial melting of the ore-related granites in the Yangchuling deposit at an average temperature of 669 °C, significantly lower than the Shimensi (774 °C), Kunshan (703 °C), and Zhuxi deposit (684 °C). This finding aligns with the parental magma in the Yangchuling deposit having higher water content, which facilitated a decompressive H_2O-saturated ascent, as evidenced by elevated $(Eu/Eu^*)/Yb_N$ ratios and their inverse relationship with zircon f_{O2} (Fig. 11d). In contrast to the H_2O-unsaturation ascent caused by dehydration melting in Zhuxi, Kunshan and Shimensi, the H_2O-saturation ascent of the relatively H_2O-rich Yangchuling magmas suggests that their melting reactions were mainly driven by water-fluxed melting (Weinberg and Hasalová, 2015).

In addition, the lack of positive correlation between Yb_N/Gd_N and Eu/Eu*, along with the significant deviation of data points from the titanite fractionation curve (Fig. 8a), indicates limited titanite co-crystallization (Loader et al., 2017). The Eu anomaly serves as an indicator of the abundance of separated plagioclase from the differentiated melt (Loucks and Fiorentini, 2023), as the impact of limited titanite co-crystallization on the Eu anomaly is minimal. The zircons of the Yangchuling granites generally exhibit a higher Eu/Eu* ratio than those of the Dahutang and Zhuxi granites (Zhang et al., 2020), suggesting a higher degree of plagioclase separation and, therefore, an origin from deeper crustal depths (Tang et al., 2024). Therefore, the significantly reduced Eu/Eu* ratio, as observed from BM granite to late-stage granites in Fig. S4, suggests crustal thinning of plagioclase-dominated crystallization at shallow depths (Tang et al., 2024). The decreased Eu/Eu* ratio

in the late-stage magma likely reflects the shift in the intraplate tectonic regime from compressional to extensional, promoting decompressive dehydration of the granitic melt. This process facilitated the exsolution of tungsten-bearing H_2O-rich fluids, contributing to the mineralization during the late magmatic stage.

5.4. H_2O-fluxed melting triggers the formation of W-rich magma

Water-fluxed melting plays a pivotal role in both the destruction of cratons and the ongoing development of an orogen, primarily by the weakening of the orogenic core or lower crust (Ge et al., 2023; Yang et al., 2022). Fluid channels form by primary faults or inherited fractures that develop from an arc-back system of crustal shortening (Dong et al., 2023), creating pathways for fluid migration (Fig. 13a). The break-off and foundering of subducted Paleo-Pacific plates led to both lateral and vertical flow of asthenosphere (Sun et al., 2024). Local heating of the thickened lower crust and subcontinental lithosphere causes the dehydration of the lithospheric roots.

Volatile and water-rich fluids are fed through the channel to the upper W-rich source region, resulting in H_2O-fluxed melting within the layer and the formation of the fertile W-rich parental magma of BM (Fig. 13a). Recirculating water released from the break-off or foundering of deep slabs and/or hydrated lithospheric roots can lower the solidus temperature of the W-rich source region, which is characterized by a low melting temperature (~690 °C, Fig. 8b and Supplementary Table S4). Furthermore, low-temperature partial melting (<750 °C) facilitates muscovite consumption, releasing W from the protolith into melts. This resolves the apparent paradox of decoupled W—Sn mineralization (Zhao et al., 2022b). Consequently, H_2O-fluxed melting of 70 % crustal materials at low temperatures promotes the generation of BM's fertile W-bearing magma (Fig. 10b). The resulting H_2O-fluxed melting plays a crucial role in the H_2O-saturated ascent and emplacement of magmas, as well as the development of local extensional tectonics (Weinberg and Hasalová, 2015). As the fault evolves into fracture walls (Fig. 13b), mantle source material is continuously supplied to the magma source region, as evidenced by the gradual increase in mantle-derived components from BM to FBG, BGP, CG and PGP (Fig. 10b). This corresponds to the evolutionary trend from 'hybrid' S-type to I-type granite from the early to late stages in the Yangchuling deposit (Fig. 9b). Similarly, the zircon $\varepsilon_{Hf}(t)$ (−1.63) and whole-rock $\varepsilon_{Nd}(t)$ (−5.17) values of the late CG granite are higher than those of the early BM granite (−1.98 and − 5.43, respectively), while the PGP granite displays the highest $\varepsilon_{Nd}(t)$ value of −5.10 (Huang et al., 2023; Mao et al., 2017). The Nd—Hf isotope evidence also suggests the incorporation of an increasing proportion of mantle-derived components in the late-stage granites. The heat and mass transfer associated with water-fluxed melting promotes the expansion of the melting region and the generation of new magma, increasingly enriched in mantle-derived components, reshaping the lithospheric roots and enhancing the extensional dynamics (Fig. 13b).

Expansion of the melting zone (Fig. 13c) triggers gravitational delamination of the thickened lower crust via density instability. The overlying layer of the delaminated terrane is further heated by the influx of mantle material, resulting in a rise in the geothermal gradient. The hydrous minerals in the overlying strata of the magma chamber of the CG granodiorite begin to dehydrate, leading to the dehydration melting in this region. In addition, the merging of ~65 % of the mantle-derived materials through inherited channels forms the parental magma of PGP and the strengthens crustal extension (Fig. 10b, Fig. 13c). The delamination further enhanced the extensional tectonic regime and influenced the flow patterns of the deep asthenosphere (Fig. 13c). Finally, in the post-delamination stage, mantle-derived material refills the void between delaminated terrane and overlying strata, enhancing the melting of the delaminated terrane to form mantle-derived parental magma of spessartite (Fig. 13d). This intrusion of synplutonic spessartite dikes clearly reflects the dynamic characteristics of the tectonic setting, where extensional forces facilitate the development of pathways for deep magma ascent, significantly extending and thinning the crust. This suggests an intraplate post-compressional extensional tectonic transition around 144 Ma in the middle segment of the JOB. The completion of the intrusion of the synplutonic spessartite dikes marks the cessation of tectonic-magmatic-hydrothermal activity in the Yangchuling deposit. This interpretation of the tectonic regime transition in the Yangchuling deposit during the Late Jurassic to Early Cretaceous is spatially and temporally consistent with the opening of the JOB intraplate window driven by the subduction of Paleo-Pacific and Izanagi plates beneath the JOB, which triggered depth-dependent extension, crustal thinning, and melting that resulted in the production of W-mineralizing granitoids at ~145–137 Ma (Dong et al., 2023; Li et al., 2014).

The trend toward I-type granite with increasing f_{O2} may be associated with a decline in magma fertility for W-mineralization. The

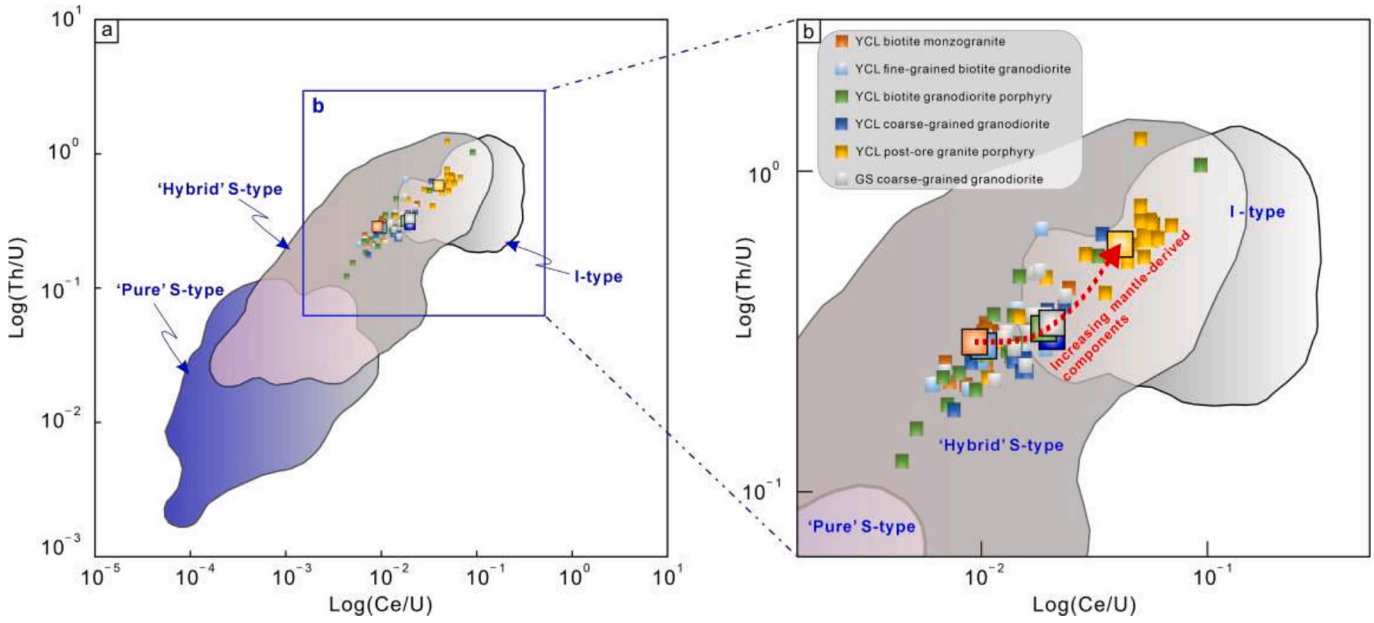

Fig. 9. Plots of Ce/U vs. Th/U for magmatic zircons of granites for the Yangchuling-Guaishan area. The distinguishing plots for I-type, hybrid S-type and pure S-type granites are based on (Roberts et al., 2024).

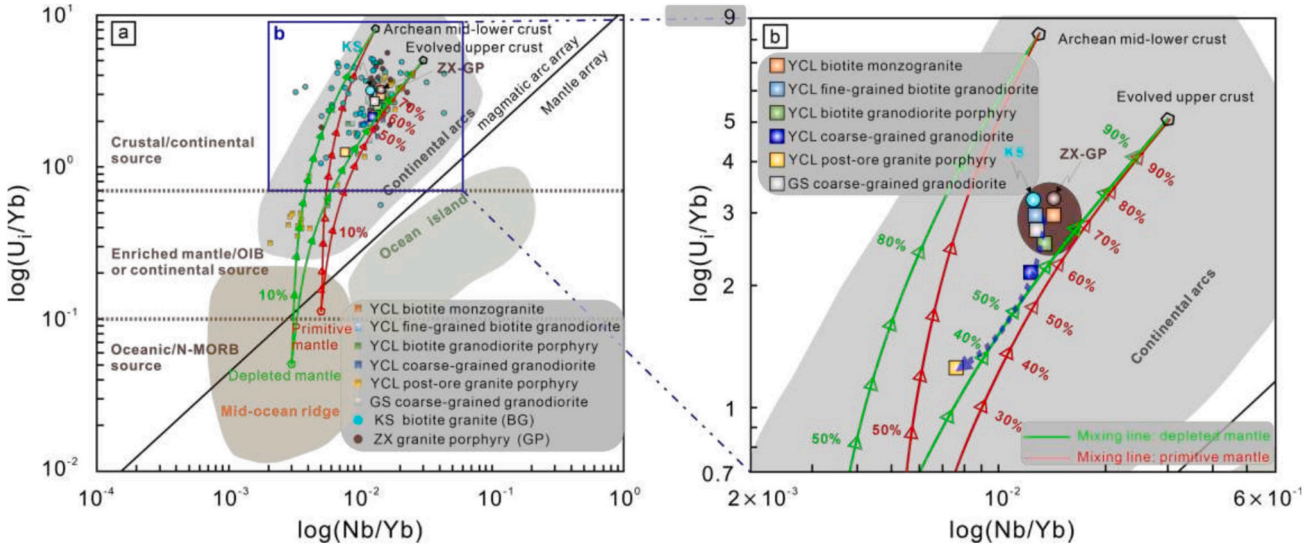

Fig. 10. Plots of U_i /Yb vs. Nb/Yb for (a) zircons from representative W—Sn deposits in the Jiangnan and (b) zircons from the Yangchuling W—Mo deposits (Grimes et al., 2015).

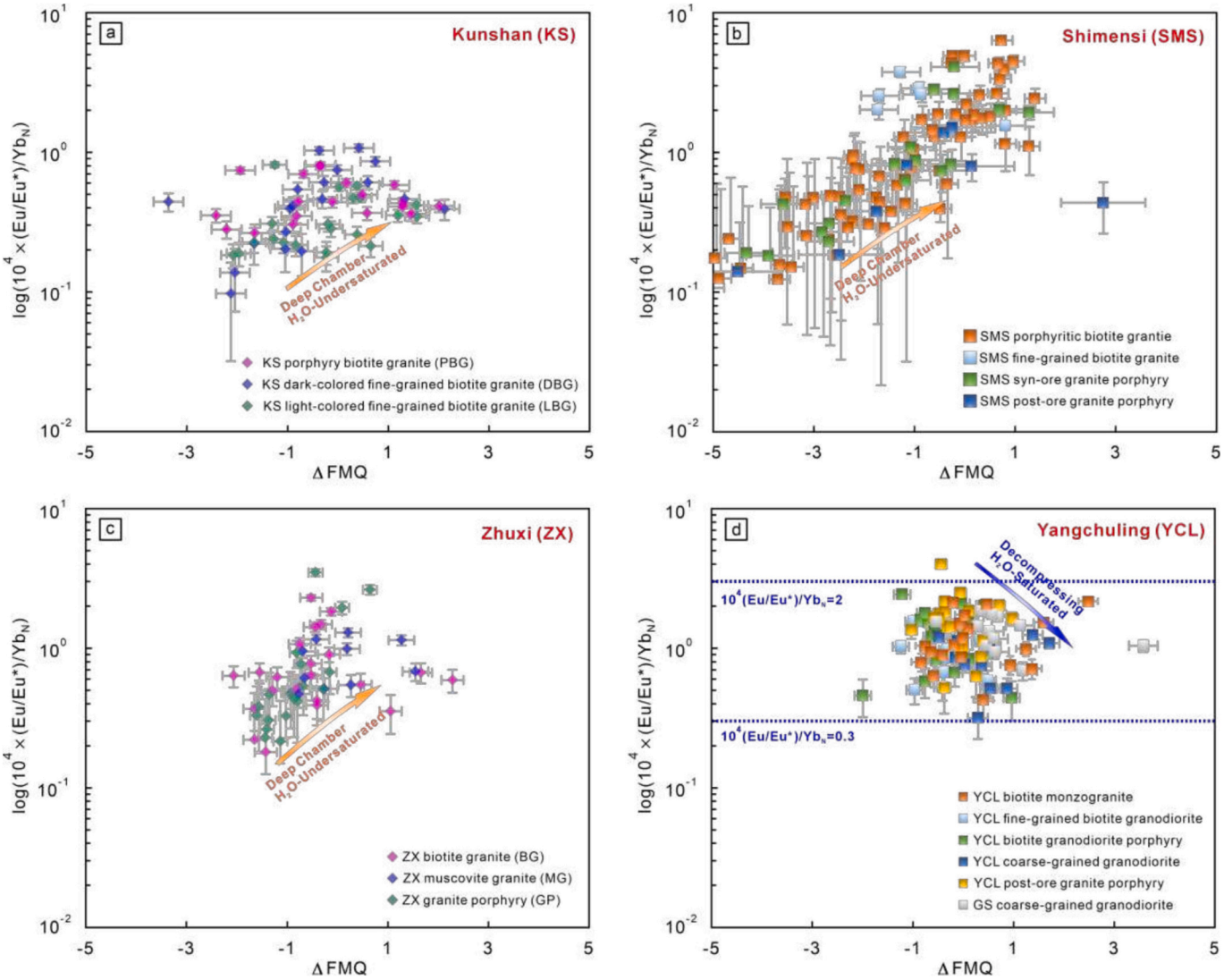

Fig. 11. Co-evolutive diagram of f_{O2} and hydration states of W-rich magma from (a) Kunshan, (b) Shimensi, (c) Zhuxi, and (d) Yangchuling during magmatic differentiation (Loucks and Fiorentini, 2023; Lu et al., 2016).

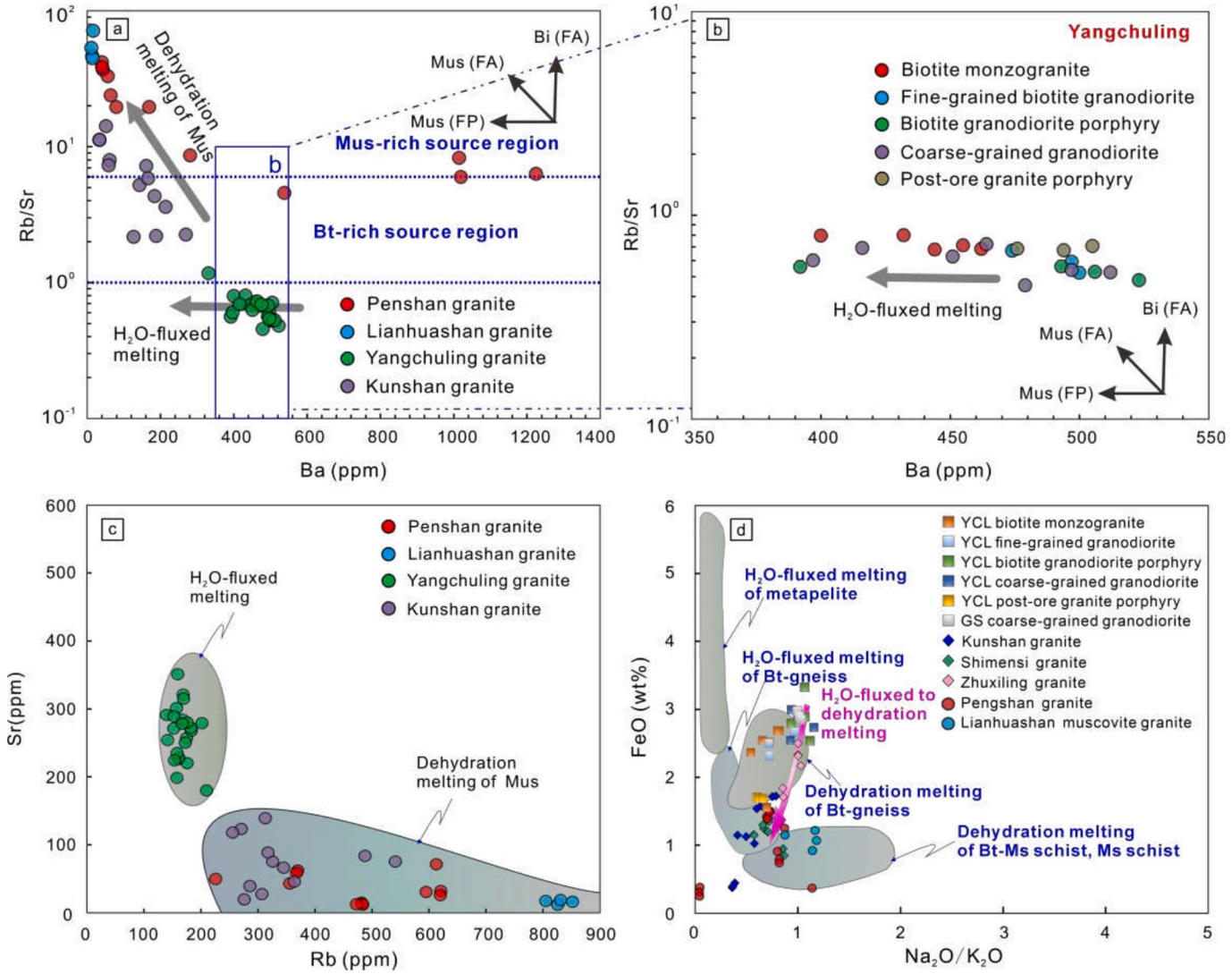

Fig. 12. (a) & (b) Ba vs. Rb/Sr, (c) Rb vs. Sr, and (d) Na_2O/K_2O vs. FeO diagrams of melt compositions for different melting reactions (Inger and Harris, 1993; Weinberg and Hasalová, 2015).

decreased grade of tungsten ore hosted in the late-stage BGP, CG and non-mineralized PGP granites in the Yangchuling deposit, along with the CG granite characterized by weak molybdenum mineralization in the Guaishan area. The increased mantle-derived contribution weakened the fertility of late-stage BGP and CG granites. In contrast, the BM and FBG granites host primary scheelite-bearing quartz-vein orebodies. The weakening of W-mineralization potential in the late-stage BGP and CG granites in the Yangchuling-Guaishan area may be attributed to the depletion of tungsten in melts caused by an increased mantle contribution, which consequently reduces the tungsten budget in the source region. In conclusion, extensional thinning of the crust reduces the residence time of ore-related melt in the crust and promotes the formation of a weakly peraluminous, moderately differentiated felsic magma with fewer volatiles in the Yangchuling deposit (Karakas and Dufek, 2015), coupled with the absence of volatile-rich alteration e.g., fluoritization and the previously mentioned whole-rock elemental properties of a weak-negative Eu anomaly and a weakly peraluminous composition, which is distinct from the volatile-rich, highly differentiated, strongly peraluminous magma found in the Dahutang and Zhuxi ore field (Song et al., 2022; Xiang et al., 2015).

6. Conclusions

Our comprehensive analysis of the in-situ elemental and U—Pb isotopes of zircons, whole-rock composition of granitoids, and *Re*—Os isotopic studies of molybdenite from the Yangchuling-Guaishan area provides robust evidence for identifying the hybrid sources of Early Cretaceous intrusions. Additionally, this study highlights a key role of water-fluxed melting in the generation of W-rich magma that was accompanied by a temporally increased proportions of mantle-derived components in the magmatic succession. thereby enhancing the understanding of tungsten mineralization.

(1) The magmas associated with large-scale W—Sn polymetallic mineralization in the JTOB are typically of high crustal derivation (~60 %–70 %).

(2) Compared to S-type W-rich granitic magma in the JTOB, the I-type granitic magma in the Yangchuling deposit was derived by water-fluxed melting, its high H_2O saturation content facilitated decompressive H_2O-saturated ascent.

(3) The early water-fluxed melting triggered the formation of a W-rich fertile magmatic succession that is characterized by lower temperature, higher content of SiO_2, a higher proportion of crustal source components and provided H_2O-saturated ascent compared to the later barren magmas.

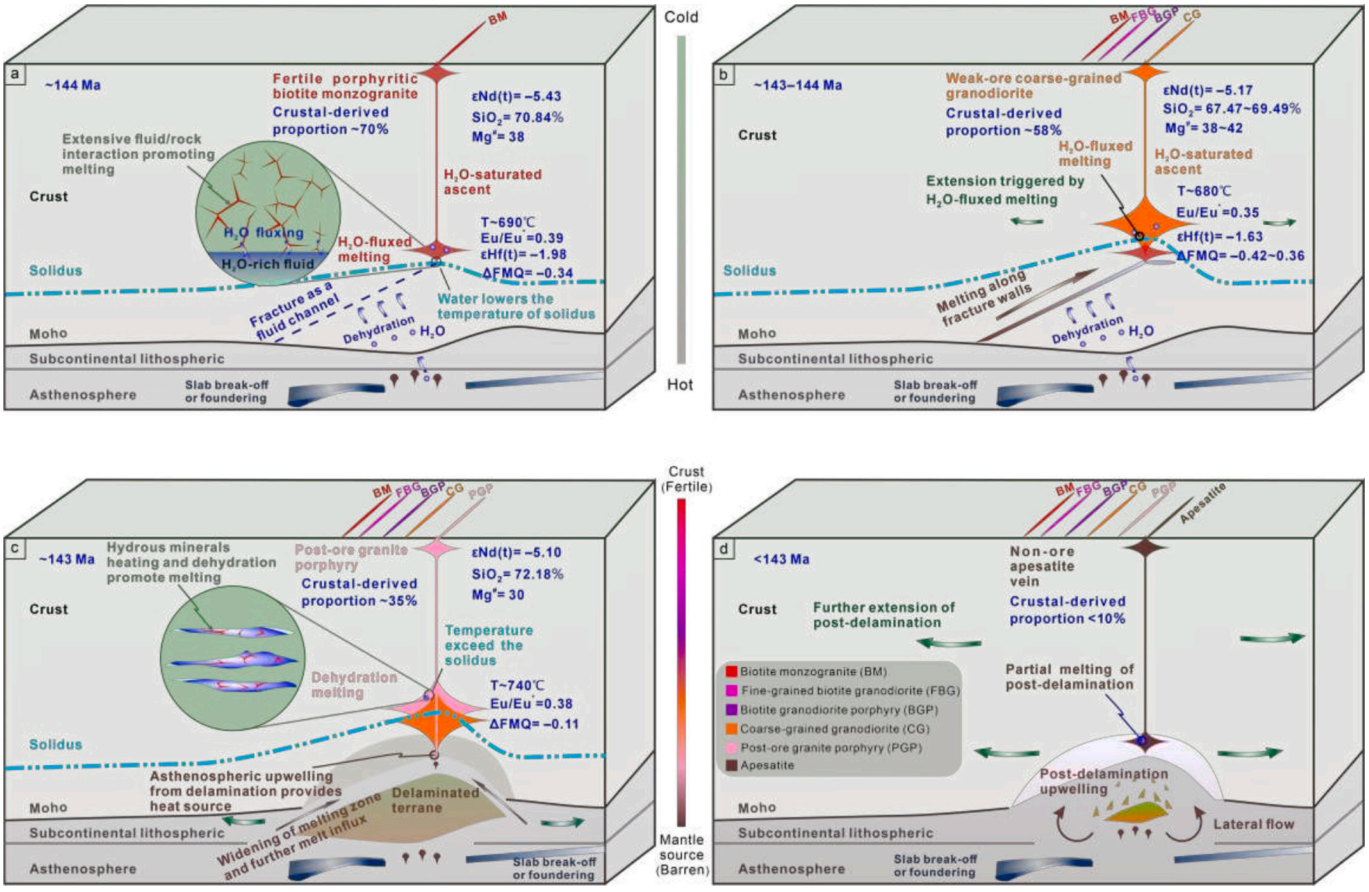

Fig. 13. The water-fluxed melt channelization & gravitational delamination (WMCGD) model and its role in generating W-rich magmas. (a) Dehydration of lithospheric roots and/or deep recirculating water released from the break-off or foundering of deep slabs, along with the release of volatiles, promote water-fluxed melting in the hot W-rich source region, forming the fertile W-rich parental magma of biotite monzogranite (BM). (b) Water-fluxed melting, lasting until the maximum volume of coarse-grained granodiorite (CG) parental magma formation , has weakened the lithospheric roots, trigging the tectonic regime of extension. This period is accompanied by an increase in mantle-derived components in the source region through fracture walls. (c) Dehydration of hydrous minerals promotes dehydration melting in the source region of post-ore granite porphyry, with limited melt volume due to restricted replenishment of hydrous phases in intraplate settings (Weinberg and Hasalová, 2015). (d) Mantle-derived material refills the void between gravitationally delaminated terrane and overlying strata, promoting melting to form mantle-derived spessartite parental magma in the post-delamination stage.

(4) The increased contribution of mantle-derived components significantly weakened the fertility of late-stage biotite granodiorite porphyry and coarse-grained granodiorite and decreasesd the tungsten budget in the source region. By integrating water-fluxed melt channelization and density-driven gravitational delamination, the WMCGD model (Water-fluxed Melt Channelization & Gravitational Delamination) explains how tungsten concentrations may be diluted through mantle material entrainment.

(5) The extensional thinning of the crust reduced the residence time of ore-related melts and promoted the formation of weakly peraluminous, moderately differentiated felsic magma with a lesser amount of volatiles in the Yangchuling deposit in Early Cretaceous time (143–144 Ma).

CRediT authorship contribution statement

Qingqing Yin: Writing – original draft, Conceptualization. **Juxing Tang:** Writing – original draft, Supervision, Methodology, Conceptualization. **Jingjing Dai:** Writing – original draft, Data curation, Conceptualization. **Inna Safonova:** Writing – review & editing, Conceptualization. **Faqiao Li:** Conceptualization, Investigation. **Hao Sun:** Investigation. **Yumin Xu:** Investigation, Data curation. **Xinkui Xiang:** Investigation, Data curation. **Jinling Xie:** Project administration, Methodology. **Baoping Gan:** Formal analysis, Investigation. **Bohao Yin:** Software, Methodology. **Zhongchao Zheng:** Investigation, Data curation. **Feng Liang:** Software, Formal analysis. **Liqiang Wang:** Project administration.

Declaration of competing interest

The authors declare that they have no known competing financial interests or personal relationships that could have appeared to influence the work reported in this paper.

Acknowledgments

We thank Rong Tan and Xian-Jun Zhou from the Jiangxi Bureau of Geology, as well as Wei Liu and Guo-Long Hu from Xiamen Tungsten Co., Ltd., for their invaluable assistance during our field investigation. We would like to express special thanks to Prof. Xian-Guang Wang for his constructive suggestions, which have greatly enhanced this study. This research was supported by the National Key Research and Development Program of China (2021YFC2900100), the Ministry of Science and Higher Education of Russia, State Assignment Project (122041400044-2), the National Science and Technology Award Reserve Project Cultivation Plan from the Science and Technology Department of Jiangxi Province (20203AEI91004), and Technology Innovation Guidance Project of Science and Technology Department of

Jiangxi Province (S2023KJSLG0007).

Appendix A. Supplementary data

Supplementary data to this article can be found online at https://doi.org/10.1016/j.lithos.2025.108197.

References

Bell, E.A., Boehnke, P., Harrison, T.M., 2016. Recovering the primary geochemistry of Jack Hills zircons through quantitative estimates of chemical alteration. Geochim. Cosmochim. Acta 191, 187–202. https://doi.org/10.1016/j.gca.2016.07.016.

Bell, E.A., Boehnke, P., Barboni, M., Harrison, T.M., 2019. Tracking chemical alteration in magmatic zircon using rare earth element abundances. Chem. Geol. 510, 56–71. https://doi.org/10.1016/j.chemgeo.2019.02.027.

Brown, M., 2013. Granite: From genesis to emplacement. Geol. Soc. Am. Bull. 125, 1079–1113. https://doi.org/10.1130/B30877.1.

Burnham, A.D., Berry, A.J., 2012. An experimental study of trace element partitioning between zircon and melt as a function of oxygen fugacity. Geochim. Cosmochim. Acta 95, 196–212. https://doi.org/10.1016/j.gca.2012.07.034.

Cao, L.M., Yuan, H.Y., Zhao, L., Zhao, M.H., Huang, M.H., Hao, T.Y., Qiu, X., 2022. Fault-controlled regional magmatism and mineral deposition in central Cathaysia—Evidence from ambient noise tomography. Sci. China Earth Sci. 52, 1764–1784 [in Chinese with English abstract]. https://doi.org/10.1360/N072021-0235.

Carrasco-Godoy, C., Campbell, I.H., Cajal, Y., 2024. Quantifying the Criteria Used to Identify Zircons from Ore-Bearing and Barren Systems in Porphyry Copper Exploration. Econ. Geol. 119, 1035–1058. https://doi.org/10.5382/econgeo.5086.

Castro, A., Patiño Douce, A.E., Corretgé, L.G., De La Rosa, J.D., El-Biad, M., El-Hmidi, H., 1999. Origin of peraluminous granites and granodiorites, Iberian massif, Spain: an experimental test of granite petrogenesis. Contrib. Mineral. Petrol. 135, 255–276. https://doi.org/10.1007/s004100050511.

Collins, W.J., Murphy, J.B., Johnson, T.E., Huang, H.-Q., 2020. Critical role of water in the formation of continental crust. Nat. Geosci. 13, 331–338. https://doi.org/10.1038/s41561-020-0573-6.

Dai, P., Mao, J., Wu, S., Xie, G., Luo, X., 2018. Multiple dating and tectonic setting of the Early Cretaceous Xianglushan W deposit, Jiangxi Province, South China. Ore Geol. Rev. 95, 1161–1178. https://doi-org-s.era.lib.swjtu.edu.cn:443/10.1016/j.oregeorev.2017.11.017.

Dong, S., Li, J., Gao, R., Cawood, P.A., Thybo, H., Johnston, S.T., Jiao, L., Zhang, Y., Wang, J., 2023. Intraplate lithospheric extension revealed by seismic reflection profiling of South China. Earth Planet. Sci. Lett. 609, 118100. https://doi.org/10.1016/j.epsl.2023.118100.

Du, A.D., Qu, W.J., Wang, D.H., Li, C., 2012. Re–Os Dating and Its Application in Ore Deposits. Geol. Publ. House 15–178 [in Chinese].

Fan, C.H., Ni, P., Wang, G.G., Zhang, K.H., Wang, G.L., Li, W.S., Cui, J.M., He, J.F., 2022. Accessory minerals U-Pb geochronology of monzogranitic porphyry in Yangchuling porphyry W-Mo deposit in northern of Jiangxi Province, South China. Mineral. Deposita 41, 35–52 [in Chinese with English abstract]. 10.16111/j.0258-7106.2022.01.003.

Ferry, J.M., Watson, E.B., 2007. New thermodynamic models and revised calibrations for the Ti-in-zircon and Zr-in-rutile thermometers. Contrib. Mineral. Petrol. 154, 429–437. https://doi.org/10.1007/s00410-007-0201-0.

Foden, J., Sossi, P.A., Wawryk, C.M., 2015. Fe isotopes and the contrasting petrogenesis of A-, I- and S-type granite. Lithos 212–215, 32–44. https://doi.org/10.1016/j.lithos.2014.10.015.

Gao, L.E., Zeng, L., Asimow, P.D., 2017. Contrasting geochemical signatures of fluid-absent versus fluid-fluxed melting of muscovite in metasedimentary sources: The Himalayan leucogranites. Geology 45, 39–42. https://doi.org/10.1130/g38336.1.

Ge, R., Wilde, S.A., Zhu, W., Zhou, T., Si, Y., 2022. Formation and evolution of Archean continental crust: A thermodynamic – geochemical perspective of granitoids from the Tarim Craton, NW China. Earth-Sci. Rev. 234, 104219. https://doi.org/10.1016/j.earscirev.2022.104219.

Ge, R.F., Wilde, S.A., Zhu, W.-B., Wang, X.L., 2023. Earth's early continental crust formed from wet and oxidizing arc magmas. Nature 623, 334–339. https://doi.org/10.1038/s41586-023-06552-0.

Grimes, C.B., Wooden, J.L., Cheadle, M.J., John, B.E., 2015. "Fingerprinting" tectono-magmatic provenance using trace elements in igneous zircon. Contrib. Mineral. Petrol. 170, 46. https://doi.org/10.1007/s00410-015-1199-3.

Hoskin, P.W.O., 2005. Trace-element composition of hydrothermal zircon and the alteration of Hadean zircon from the Jack Hills, Australia. Geochim. Cosmochim. Acta 69, 637–648. https://doi.org/10.1016/j.gca.2004.07.006.

Huang, Y., Huang, X.D., Lu, J.J., Zhang, R.Q., Wu, J.W., Yan, J.C., 2023. Petrogenesis of granite porphyry in the Yangchuling tungsten ore district, northern Jiangxi. Geol. J. China Univ. 29, 795–808 [in Chinese with English abstract]. 10.16108/j.issn1006-7493.2022049.

Inger, S., Harris, N., 1993. Geochemical Constraints on Leucogranite Magmatism in the Langtang Valley, Nepal Himalaya. J. Petrol. 34, 345–368. https://doi.org/10.1093/petrology/34.2.345.

Jiang, W.C., Li, H., Mathur, R., Wu, J.-H., 2019. Genesis of the giant Shizhuyuan W–Sn–Mo–Bi–Pb–Zn polymetallic deposit, South China: Constraints from zircon geochronology and geochemistry in skarns. Ore Geol. Rev. 111, 102980. https://doi.org/10.1016/j.oregeorev.2019.102980.

Karakas, O., Dufek, J., 2015. Melt evolution and residence in extending crust: Thermal modeling of the crust and crustal magmas. Earth Planet. Sci. Lett. 425, 131–144. https://doi.org/10.1016/j.epsl.2015.06.001.

Li, J., Zhang, Y., Dong, S., Johnston, S.T., 2014. Cretaceous tectonic evolution of South China: A preliminary synthesis. Earth-Sci. Rev. 134, 98–136. https://doi.org/10.1016/j.earscirev.2014.03.008.

Liu, Y., Hu, Z., Gao, S., Günther, D., Xu, J., Gao, C., Chen, H., 2008. In situ analysis of major and trace elements of anhydrous minerals by LA-ICP-MS without applying an internal standard. Chem. Geol. 257, 34–43. https://doi.org/10.1016/j.chemgeo.2008.08.004.

Loader, M.A., Wilkinson, J.J., Armstrong, R.N., 2017. The effect of titanite crystallisation on Eu and Ce anomalies in zircon and its implications for the assessment of porphyry Cu deposit fertility. Earth Planet. Sci. Lett. 472, 107–119. https://doi.org/10.1016/j.epsl.2017.05.010.

Loucks, R.R., Fiorentini, M.L., 2023. Oxidation of magmas during gain and loss of H2O recorded by trace elements in zircon. Earth Planet. Sci. Lett. 622, 118377. https://doi.org/10.1016/j.epsl.2023.118377.

Loucks, R.R., Fiorentini, M.L., Henríquez, G.J., 2020. New magmatic oxybarometer using trace elements in zircon. J. Petrol. 61, egaa034. https://doi.org/10.1093/petrology/egaa034.

Loucks, R.R., Henríquez, G.J., Fiorentini, M.L., 2024. Zircon and Whole-Rock Trace Element Indicators of Magmatic Hydration State and Oxidation State Discriminate Copper Ore-Forming from Barren Arc Magmas. Econ. Geol. 119, 511–523. https://doi.org/10.5382/econgeo.5071.

Lu, Y.J., Loucks, R.R., Fiorentini, M., McCuaig, T.C., Evans, N.J., Yang, Z.M., Hou, Z.Q., Kirkland, C.L., Parra-Avila, L.A., Kobussen, A., 2016. Zircon Compositions as a Pathfinder for Porphyry Cu ± Mo ± Au Deposits, in: Tectonics and Metallogeny of the Tethyan Orogenic Belt. Soc. Econ. Geologists. https://doi.org/10.5382/SP.19.13.

Mao, J.W., Zhang, Z.C., Zhang, Z.H., Du, A.D., 1999. Re-Os isotopic dating of molybdenites in the Xiaoliugou W (Mo) deposit in the northern Qilian mountains and its geological significance. Geochim. Cosmochim. Acta 63, 1815–1818. https://doi.org/10.1016/S0016-7037(99)00165-9.

Mao, J.W., Xiong, B.K., Liu, J., Pirajno, F., Cheng, Y., Ye, H., Song, S., Dai, P., 2017. Molybdenite Re/Os dating, zircon U–Pb age and geochemistry of granitoids in the Yangchuling porphyry W–Mo deposit (Jiangnan tungsten ore belt), China: Implications for petrogenesis, mineralization and geodynamic setting. Lithos 286–287, 35–52. https://doi.org/10.1016/j.lithos.2017.05.023.

Mao, J.W., Wu, S.H., Song, S.W., Dai, P., Xie, G.Q., Su, Q.W., Liu, P.P., Wang, X.G., Yu, Z. Z., Chen, X.Y., Tang, W.X., 2020. The world-class Jiangnan tungsten belt: Geological characteristics, metallogeny, and ore deposit model. Chin. Sci. Bull. 65, 3746–3762 [in Chinese with English abstract]. https://doi.org/10.1360/TB-2020-0370.

Mole, D.R., Thurston, P.C., Marsh, J.H., Stern, R.A., Ayer, J.A., Martin, L.A.J., Lu, Y.J., 2021. The formation of Neoarchean continental crust in the south-east Superior Craton by two distinct geodynamic processes. Precambrian Res. 356, 106104. https://doi.org/10.1016/j.precamres.2021.106104.

Nathwani, C., Blundy, J., Large, S.J.E., Wilkinson, J.J., Buret, Y., Loader, M.A., Tavazzani, L., Chelle-Michou, C., 2024. A zircon case for super-wet arc magmas. Nat. Commun. 15, 8982. https://doi.org/10.1038/s41467-024-52786-5.

Roberts, N.M.W., Yakymchuk, C., Spencer, C.J., Keller, C.B., Tapster, S.R., 2024. Revisiting the discrimination and distribution of S-type granites from zircon trace element composition. Earth Planet. Sci. Lett. 633, 118638. https://doi.org/10.1016/j.epsl.2024.118638.

Romer, R.L., Kroner, U., 2016. Phanerozoic tin and tungsten mineralization—Tectonic controls on the distribution of enriched protoliths and heat sources for crustal melting. Gondwana Res. 31, 60–95. https://doi.org/10.1016/j.gr.2015.11.002.

Roy, J.K., Naik, A., Bhattacharya, S., 2024. Insights into the anatectic origin of granites parental to tungsten mineralization: A case study from the trans-Aravalli terrane, NW India. Resour. Geol. 74, e12327. https://doi.org/10.1111/rge.12327.

Samperton, K.M., Schoene, B., Cottle, J.M., Keller, C.B., Crowley, J.L., Schmitz, M.D., 2015. Magma emplacement, differentiation and cooling in the middle crust: Integrated zircon geochronological–geochemical constraints from the Bergell Intrusion, Central Alps. Chem. Geol. 417, 322–340. https://doi.org/10.1016/j.chemgeo.2015.10.024.

Sant Ovaia, H., Cruz, C., Gonçalves, A., Noronha, F., 2021. Reduced- or Ilmenite-type Granites Versus Oxidized- or Magnetite-type Granites: Occurrence in Iberian Variscan Belt. https://doi.org/10.5194/egusphere-egu21-11885.

Shen, H.F., Li, L.X., Li, H.M., Li, X.S., Sun, X.Y., Wen, Y.Z., Li, W.C., Meng, Y.H., 2022. Control of the large-sized Mesozoic W-Sn mineralization in southern Hunan: Insights from zircon geochronology and trace element geochemistry. Geol. Bull. China 41, 461–512 [in Chinese with English abstract]. 10.12097/j.issn.1671-2552.2022.2-3.024.

Smythe, D.J., Brenan, J.M., 2015. Cerium oxidation state in silicate melts: Combined fO2, temperature and compositional effects. Geochim. Cosmochim. Acta 170, 173–187. https://doi.org/10.1016/j.gca.2015.07.016.

Song, S., Mao, J., Yuan, S., Jian, W., 2022. Decoupling of Sn and W mineralization in a highly fractionated reduced granitic magma province: a case study from the Youjiang basin and Jiangnan tungsten belt. Mineral. Deposita 57, 1251–1267. https://doi.org/10.1007/s00126-022-01094-3.

Song, S., Mao, J., Romer, R.L., Jian, W., 2023. The petrogenesis of the Yangchuling porphyry W-Mo deposit, South China, an oxidized tungsten systems. Contrib. Mineral. Petrol. 178, 39. https://doi.org/10.1007/s00410-023-02023-x.

Song, W., Yao, J., Chen, H., Sun, W., Lai, C., Xiang, X., Luo, X., Jourdan, F., 2018. A 20 m.y. long-lived successive mineralization in the giant Dahutang W–Cu–Mo deposit. South China. Ore Geol. Rev. 95, 401–407. https://doi.org/10.1016/j.oregeorev.2018.02.033.

Stein, H.J., Markey, R.J., Morgan, J.W., Hannah, J.L., Scherstén, A., 2001. The remarkable Re–Os chronometer in molybdenite: how and why it works. Terra Nova 13, 479–486. https://doi.org/10.1046/j.1365-3121.2001.00395.x.

Sun, L., Zhang, Y., Sun, Z., Miao, X., Li, R., Zhang, W., 2024. Origin of the Site U1504 alkaline basalts in the South China Sea continental margin: Insights on deep mantle diversity and subduction dynamics under continental arcs. Geol. Soc. Am. Bull. 136, 5027–5038. https://doi.org/10.1130/B37471.1.

Sun, S.S., McDonough, W.F., 1989. Chemical and isotopic systematics of oceanic basalts: implications for mantle composition and processes. Geol. Soc. Lond. Spec. Publ. 42, 313–345. https://doi.org/10.1144/GSL.SP.1989.042.01.1.

Sylvester, P.J., 1998. Post-collisional strongly peraluminous granites. Lithos 45, 29–44. https://doi.org/10.1016/s0024-4937(98)00024-3.

Tang, M., Guo, Z., Cao, W., Chu, X., 2024. Revisiting zircon Eu anomaly as a proxy for crustal thickness: A case study of the Sierra Nevada Batholith. Earth Planet. Sci. Lett. 643, 118897. https://doi.org/10.1016/j.epsl.2024.118897.

Trail, D., Watson, E.B., Tailby, N.D., 2012. Ce and Eu anomalies in zircon as proxies for the oxidation state of magmas. Geochim. Cosmochim. Acta 97, 70–87. https://doi.org/10.1016/j.gca.2012.08.032.

Vermeesch, P., 2018. Isoplot R: A free and open toolbox for geochronology. Geosci. Front. 9, 1479–1493. https://doi.org/10.1016/j.gsf.2018.04.001.

Wang, X.G., Cao, S.H., Gong, L.X., Hu, Z.H., Cao, M.X., Zhang, D.F., Chen, Q.R., 2023. Tungsten-tin polymetallic metallogenic series and prospecting in Jiangxi Province. Acta Geosci. Sin. 44, 916–932 [in Chinese with English abstract]. https://doi.org/10.3975/cagsb.2022.112301.

Wang, Y., Fan, W., Guo, F., Peng, T., Li, C., 2003. Geochemistry of Mesozoic Mafic Rocks Adjacent to the Chenzhou-Linwu fault, South China: Implications for the Lithospheric Boundary between the Yangtze and Cathaysia Blocks. Int. Geol. Rev. 45, 263–286. https://doi.org/10.2747/0020-6814.45.3.263.

Weinberg, R.F., Hasalová, P., 2015. Water-fluxed melting of the continental crust: A review. Lithos 212–215, 158–188. https://doi.org/10.1016/j.lithos.2014.08.021.

Xiang, X.K., Wang, P., Sun, D.M., Zhong, B., 2013. Re-Os isotopic age of molybdenite from the Shimensi tungsten polymetallic deposit in northern Jiangxi province and its geological implications. Geol. Bull. China 32, 1824–1831 [in Chinese with English abstract]. https://doi.org/10.3969/j.issn.1671-2552.2013.11.015.

Xiang, X.K., Yin, Q.Q., Sun, K.K., Chen, B., 2015. Origin of the Dahutang syn-collisional granite-porphyry in the middle segment of the Jiangnan orogen: zircon U-Pb geochronologic, geochemical and Nd-Hf isotopic constraints. Acta Petrol. Mineral. 34, 581–600 [in Chinese with English abstract]. https://doi.org/10.3969/j.issn.1000-6524.2015.05.001.

Xu, Y.M., Wang, T.C., Wang, W.F., Yin, Q.Q., Xiang, X.K., 2023. Genesis of Yanshanian magmatic rocks in Yangchuling tungsten polymetallic deposits in the eastern Jiangnan Orogenic Belt. China Tungsten Ind. 38, 8–21 [in Chinese with English abstract]. https://doi.org/10.3969/j.issn.1009-0622.2023.02.002.

Yang, C., Xu, Y., Xia, X., Yang, J., Sun, J., Zhang, W., Yang, Q., Yang, Y., 2022. High Water contents in zircons suggest water-fluxed crustal melting during cratonic destruction. Geophys. Res. Lett. 49, e2021GL097126. https://doi.org/10.1029/2021GL097126.

Yin, Q.Q., Xiang, X.K., Yu, Z.D., Yang, X.F., Wang, T.C., Zhong, B., Tan, R., Liao, J.H., Zhu, Y.S., 2020. Genesis of S-type Granites in the Pengshan Sn-polymetallic ore field, northern Jiangxi Province and its implications. Acta Geol. Sin. - Engl. Ed. 94, 1860–1873. https://doi.org/10.1111/1755-6724.14599.

Yin, Q.Q., Tang, J.X., Xiang, X.K., Xie, J.L., Dai, J.J., Peng, B., 2024. Petrogenesis of reductive S-type granites in the Pengshan district, northern Jiangxi Province, and their implications for tin enrichment: Insights from zircon trace elements. Earth Sci. Front. 31, 133–149 [in Chinese with English abstract]. 10.13745/j.esf.sf.2023.9.3.

Yin, Q.Q., Tang, J.X., Pei, Q.M., Safonova, I., Xiang, X.K., Dai, J.J., Zhou, A., Lin, B., Xu, Y., Yu, Z.D., Xie, J.L., Lin, R.H., Peng, B., Wang, L.Q., 2025. A vertical reverse zoning in the Kunshan W-Mo-Cu deposit, South China: Insights from mineral paragenesis, zircon geochemistry and S-Pb-O isotopes. Gondwana Res. 142, 236–251. https://doi.org/10.1016/j.gr.2025.03.004.

Yuan, S., Williams-Jones, A.E., Romer, R.L., Zhao, P.L., Mao, J., 2019. Protolith-Related Thermal Controls on the Decoupling of Sn and W in Sn-W Metallogenic Provinces: Insights from the Nanling Region, China. Econ. Geol. 114, 1005–1012. https://doi.org/10.5382/econgeo.4669.

Zeng, Q.Q., Hu, Z.H., Wang, X.G., Gong, L.X., Nie, L.M., Li, Q., 2019. Geochronology of the Yangchuling tungsten-molybdenum depoist in Duchang County, Jiangxi Province. Geol. China 46, 841–849 [in Chinese with English abstract]. 10.12029/gc20190414.

Zhang, A., Sun, T., Tan, S., Li, W., Liu, Z., Zhou, J., Tang, M., 2021. Geochronology, geochemistry and oxidation state of the Dongyuan biotite granite in the Jiangnan tungsten ore belt: Implications for the I-type granite-related W mineralization. Ore Geol. Rev. 133, 104080. https://doi.org/10.1016/j.oregeorev.2021.104080.

Zhang, W., Jiang, S.-Y., Gao, T., Ouyang, Y., Zhang, D., 2020. The effect of magma differentiation and degassing on ore metal enrichment during the formation of the world-class Zhuxi W-Cu skarn deposit: Evidence from U-Pb ages, Hf isotopes and trace elements of zircon, and whole-rock geochemistry. Ore Geol. Rev. 127, 103801. https://doi.org/10.1016/j.oregeorev.2020.103801.

Zhao, P.L., Chu, X., Williams-Jones, A.E., Mao, J., Yuan, S., 2022a. The role of phyllosilicate partial melting in segregating tungsten and tin deposits in W-Sn metallogenic provinces. Geology 50, 121–125. https://doi.org/10.1130/G49248.1.

Zhao, P.L., Zajacz, Z., Tsay, A., Yuan, S., 2022b. Magmatic-hydrothermal tin deposits form in response to efficient tin extraction upon magma degassing. Geochim. Cosmochim. Acta 316, 331–346. https://doi.org/10.1016/j.gca.2021.09.011.